iScience

CellPress

Article

Enhancer-Driven Gene Expression (EDGE) Enables the Generation of Viral Vectors Specific to Neuronal Subtypes

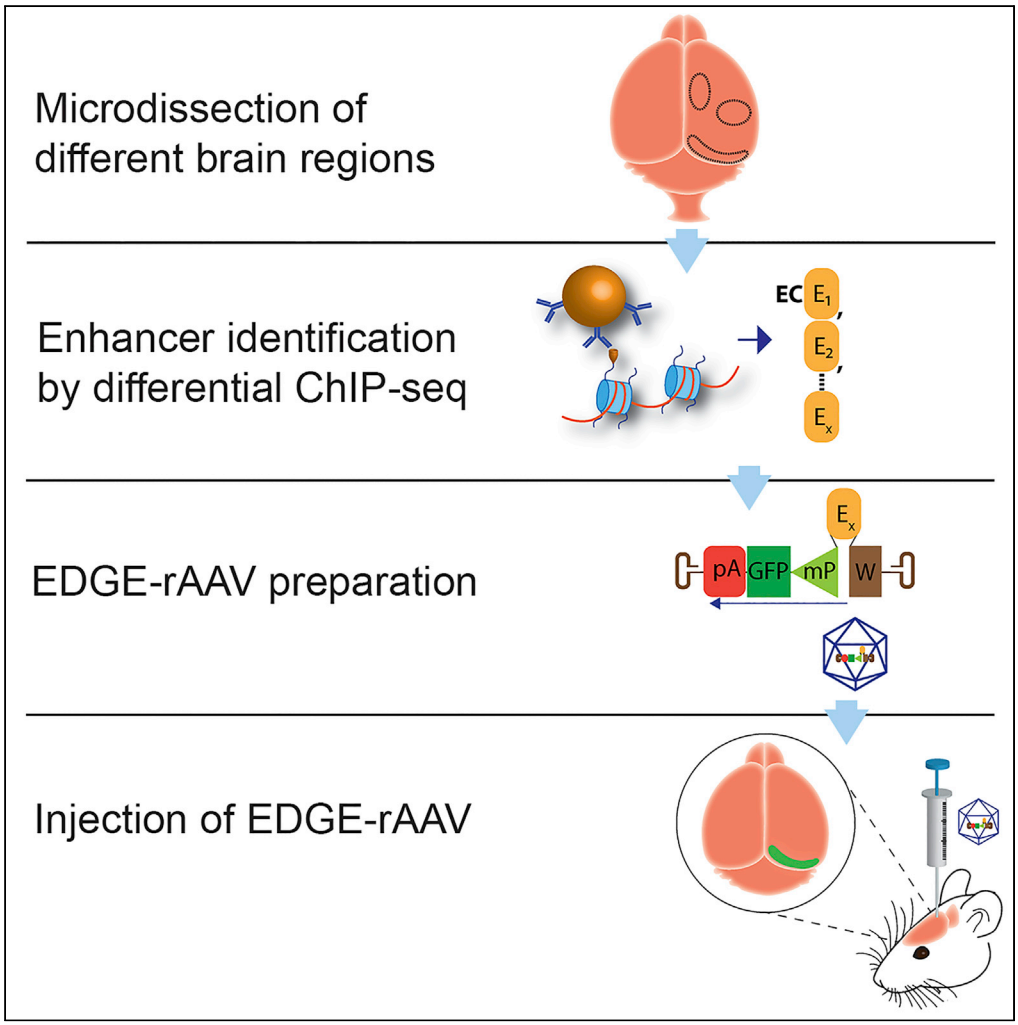

Rajeevkumar Raveendran Nair, Stefan Blankvoort, Maria Jose Lagartos, Cliff Kentros

clifford.kentros@ntnu.no

HIGHLIGHTS

rAAVs with enhancers unique to a brain region specify cell types of that brain region

This requires viral constructs optimized to express only with enhancers

One rAAV distinguishes distinct subtypes of excitatory neurons in a cortical layer

The same specificity is seen in wild-type animals of at least two species

Nair et al., iScience *23*, 100888 March 27, 2020
https://doi.org/10.1016/j.isci.2020.100888

iScience

CellPress

Article

Enhancer-Driven Gene Expression (EDGE) Enables the Generation of Viral Vectors Specific to Neuronal Subtypes

Rajeevkumar Raveendran Nair,[1] Stefan Blankvoort,[1] Maria Jose Lagartos,[1] and Cliff Kentros[1,2,3,*]

SUMMARY

Although a variety of remarkable molecular tools for studying neural circuits have recently been developed, the ability to deploy them in particular neuronal subtypes is limited by the fact that native promoters are almost never specific enough. We recently showed that one can generate transgenic mice with anatomical specificity surpassing that of native promoters by combining enhancers uniquely active in particular brain regions with a heterologous minimal promoter, an approach we call EDGE (Enhancer-Driven Gene Expression). Here we extend this strategy to the generation of viral (rAAV) vectors, showing that some EDGE rAAVs can recapitulate the specificity of the corresponding transgenic lines in wild-type animals, even of another species. This approach thus holds the promise of enabling circuit-specific manipulations in wild-type animals, not only enhancing our understanding of brain function, but perhaps one day even providing novel therapeutic avenues to approach disorders of the brain.

INTRODUCTION

The mammalian brain is the most complex biological structure known, with innumerable distinct cell types differing in cytoarchitecture, electrophysiological properties, gene expression, and connectivity (Luo et al., 2008; Zeng and Sanes, 2017). Understanding brain function requires understanding neural circuits at the level of specificity at which they operate. Recent years have seen the development of truly revolutionary molecular tools that allow neuroscientists to elucidate precise neural connectivity (Callaway and Luo, 2015) and monitor (Chen et al., 2013) and manipulate (Boyden et al., 2005; Roth, 2016; Sternson and Roth, 2014) neural activity. However, optimal use of these tools to examine the functional circuitry of the brain requires the ability to deliver them specifically to particular elements of neural circuits (i.e., neuronal cell types), rather than as a nonspecific bolus affecting all of the neurons in a brain area. The use of molecular genetics is the only method by which one can perform truly cell-type specific manipulations, as evidenced by a variety of studies using transgenic animals expressing transgenes from neuronal promoters (genomic regions just upstream of the transcriptional start site) (Kanter et al., 2017; Miao et al., 2017). However, such approaches are limited by the fact that, because individual genes are expressed in a variety of cell types in the brain, promoters are not specific to a single neuronal cell type. Although estimates vary (ENCODE Project Consortium, 2012), there are at least an order of magnitude more cis-regulatory elements (i.e., enhancers and repressors, distal genomic regions that help regulate where and when promoters transcribe DNA) than promoters, suggesting that enhancers may be more specific. This led us to take an approach to the generation of molecular genetic tools that we call Enhancer-Driven Gene Expression (EDGE), based on identifying the cis-regulatory elements uniquely active in particular brain regions and combining them with a heterologous minimal promoter. When we used this strategy to make transgenic mice, they were indeed significantly more specific than the presumed parent gene, often driving expression primarily in particular sets of neurons in the brain region they were derived from (Blankvoort et al., 2018).

However, although transgenic animals are powerful tools for the analysis of neural circuits, they have limitations. They are costly in both time and resources, can be subject to insertional effects (Matthaei, 2007; Feng et al., 2000), and are most practical in a limited number of species. Moreover, although they are often excellent models of disease, transgenic technologies are far from therapeutic applications. Recombinant adeno-associated viral vectors (rAAVs) can overcome many of the above issues. They can be made relatively quickly, generally do not insert into the genome or replicate, and can be used in a variety of species (Watakabe et al., 2015) including humans and therefore have clinical potential as well (Bouard et al., 2009;

[1]Kavli Institute for Systems Neuroscience and Centre for Neural Computation, NTNU, Norway

[2]Institute of Neuroscience, University of Oregon, Eugene OR, USA

[3]Lead Contact

*Correspondence: clifford.kentros@ntnu.no

https://doi.org/10.1016/j.isci.2020.100888

Dias et al., 2018; Kotterman and Schaffer, 2014; Mendell et al., 2017). However, efforts to generate cell-specific viral vectors by capsid modifications (Koerber et al., 2008, 2009, Klimczak et al., 2009) or using promoters (Delzor et al., 2012; Kugler et al., 2003; Shevtsova et al., 2005) have been largely unsuccessful to date to address a particular cell type, with a few notable exceptions (Dimidschstein et al., 2016; Hartl et al., 2017), and even those are likely to have multiple subclasses. This is in large part because the relatively small payload size of rAAVs puts most native promoters out of reach. However, most enhancers are much smaller than promoters, raising the intriguing possibility of targeting specific neuronal cell types in any species by adapting EDGE to viral vectors, provided the background expression of the viral backbone and promoter can be minimized. Toward this end, we present results demonstrating enhancer-based viral vectors that specifically express in particular neurons of the entorhinal cortex (EC) in two different species of wild-type animals.

RESULTS

Optimization of rAAV Design for Enhancer-Driven Gene Expression

Because one can obtain some degree of apparent specificity with rAAVs by means other than transcriptional regulation, we took steps to ensure that any observed specificity comes from the enhancer element used. Most notably, AAV serotypes exhibit distinct tropisms for different cell types: for instance, AAV8 is most efficient for oligodendrocytes and astrocytes (Aschauer et al., 2013; Hutson et al., 2012) and AAV 1, 2, 5, 7, 8, 9 prefer neurons (Aschauer et al., 2013; Castle et al., 2016; Davidson et al., 2000; During et al., 2003) (although they are by no means exclusive to them), whereas rAAV9 appears well suited for cortical neurons (Aschauer et al., 2013) and a variety of AAVs with engineered capsids show specific tropisms (Deverman et al., 2016; Tervo et al., 2016). We therefore used a single serotype (AAV2/1) with a wide tropism for neurons (Hauck et al., 2003) for the vast majority of our efforts toward engineering rAAVs transcriptionally specific to particular subtypes of neurons. We selected AAV 2/1, a chimera between capsid-1 (less efficient neuronal transduction [Castle et al., 2016]) and capsid-2 (vast tropism [Wang et al., 2003]) because of its broad transduction efficiency (Hauck et al., 2003) and to prepare viruses with high purity (During et al., 2003; Mcclure et al., 2011) via heparin columns (see Transparent Methods).

Because injections of small volumes of rAAVs can appear specific because of the specific parcellation around the injection site, we used a medial entorhinal cortex (MEC) enhancer (MEC13-53) known to be specific to a particular subset of neurons in the entorhinal cortex (Blankvoort et al., 2018) in transgenic animals so we knew what to look for. Figure 1A shows the expression pattern obtained from crossing one of the MEC13-53 tTA driver lines to a payload line expressing the helper transgenes for the ΔG-rabies monosynaptic tracing system (Blankvoort et al., 2018). Expression in this cross was limited to Reelin-positive (RE+), Calbindin-negative (CB-) excitatory projection neurons in layer (LII) of the EC (Kitamura et al., 2014; Varga et al., 2010; Witter et al., 2017). Finally, we injected the same large (400 nL in mice, as opposed to the ~50-nL injections typically used with nonspecific rAAVs) volume of each virus into multiple animals using the same EC coordinates and compared only green fluorescent protein (GFP)-expressing rAAVs of similar titer (see Table S1 and Transparent Methods). For the purposes of comparison, Figure 1B shows the widespread strong expression throughout the various layers of the entorhinal cortex (as well as subiculum and parasubiculum) resulting from injecting a control AAV with a relatively (it has been shown to prefer neurons) nonspecific cytomegalovirus promoter (CMV-rAAV) of the same serotype and similar titer.

The initial step in obtaining viruses capable of driving expression as specific as the EDGE transgenic animals in wild-type brains is to find a minimal viral promoter that is capable of robust expression *only* when paired with a heterologous enhancer. This is complicated by the fact that the viral inverted terminal repeats (ITRs) themselves have transcriptional activity (Carter et al., 1993; Flotte et al., 1993; Haberman et al., 2000), as can be seen by the very weak (but still above autofluorescence) nonspecific expression obtained from a viral construct with neither a promoter nor an enhancer (Figure 1C). Note that the expression levels in Figure 1C are far below those seen with the other viruses: each panel in Figure 1 has been differentially post-acquisition processed to aid visualization, the "background" expression seen in Figure 1C would otherwise be imperceptible (see Figure S1 for comparison of each image with the same processing). To minimize this issue, we reversed the orientation of the expression cassette relative to the ITRs such that the sense strand was under the influence of the 3′ ITR, which we attenuated by putting WPRE (Zufferey et al., 1999) between the 3′ITR and the enhancer (see schematics in 1C, D). The substantial reduction in background expression enabled us to recapitulate MEC LII-specific expression in a wild-type mouse (Figure 1D) with a mutated minimal CMV promoter (CMV*) (Loew et al., 2010). Roughly similar results varying in amount

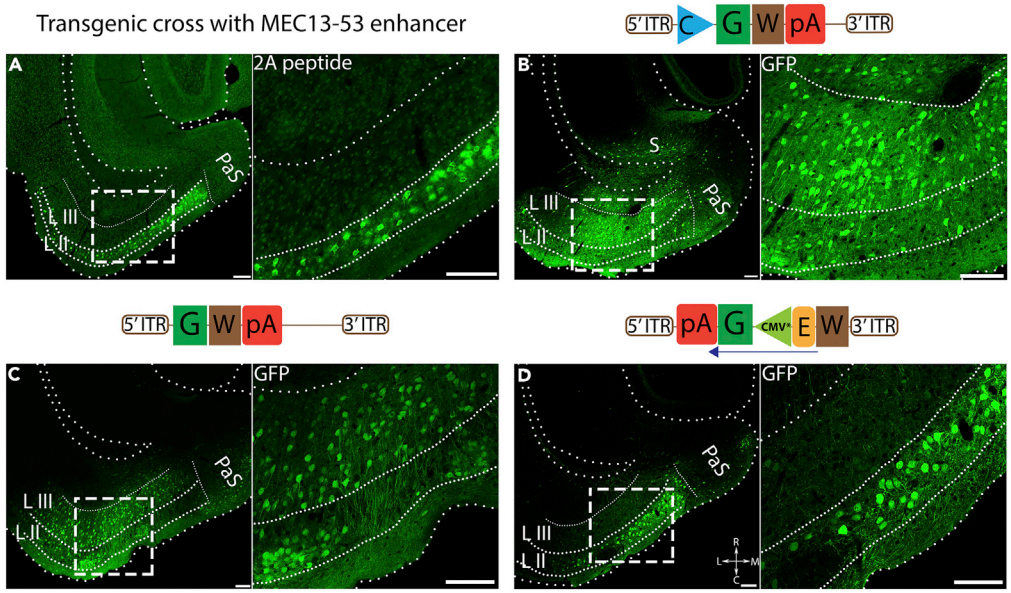

Figure 1. Optimization of rAAV Constructs for Enhancer-Dependent Gene Expression

(A) Transgene expression in a MEC13-53 tTA X tetO-TVAG transgenic cross visualized by anti-2A immunostaining is restricted to RE + LII projection neurons in EC (Blankvoort et al., 2018). Since this is a different antibody, this is purely a qualitative comparison.

(B) Injection of a nonspecific (CMV-rAAV) virus into the EC shows broad label throughout the entire region, including all layers of EC, as well as subiculum (S) and parasubiculum (PaS).

(C) The same construct without a minimal promoter shows weak nonspecific expression throughout the region that would not be visible at normal image settings (see Figure S1).

(D) Changing the orientation of the expression cassette leads to a marked reduction in nonspecific expression of MEC13-53 rAAV (see inset in [C] and [D], note that most of the LIII label in [D] is not cellular, unlike in [C], and when it is, it is very light, i.e., from baseline transcription). All murine injections were 400 nL. NB: images were differentially modified to best visualize the GFP expression pattern in each panel; comparisons of these images with the same post-acquisition settings are shown in Figure S1 (see Transparent Methods). Note that all label above background auto-fluorescence was treated as positive, even though there were two markedly distinct intensities of label. See also related Figures S1 and S2. Schematics of the viral designs are depicted on top of the corresponding image. ITR, inverted terminal repeat; W, woodchuck hepatitis virus post-transcriptional regulatory element; pA, human growth hormone polyadenylation signal; E, enhancer; G, Green fluorescent protein; C, cytomegalovirus promoter; CMV*, mutated minimal cytomegalovirus promoter. Scale bar, 100 μm.

and specificity were obtained with other minimal promoters (Figure S2), but we selected CMV* for all subsequent experiments (and hereafter simply refer to the enhancer) as it was the smallest one that worked well. The specificity of the expression of this virus as compared with a nonspecific CMV-rAAV virus is quantified in Figure 2. Although still clearly far more specific than the CMV-rAAV, the quantification of MEC13-53 rAAV does not seem as specific as it looks in the figure panels because in our counts we did not distinguish between weak "background" label (such as that seen in Figures 1C and S1 without a promoter) and the strong specific labeling (see below).

MEC13-53 EDGE rAAVs Express Specifically in Layer II Stellate Cells in Wild-Type Mice and Rats

The neuron-specific stain NeuN (Boccara et al., 2015) confirms the robust LII-specific expression of the MEC13-53 rAAV (Figures S3A and S3C) in neurons (100% of labeled cells were NeuN+, data not shown). Weak, "background" GFP expression was observed in other layers as well in both this virus (Figure S3A, inset) and in the rAAV backbone (i.e., the same virus lacking the enhancer, Figure S3B, inset), which in contrast did not strongly label any cells. Within LII of MEC there are two major classes of excitatory principal neurons, RE + stellate cells and CB + pyramidal cells (Rowland et al., 2018; Witter et al., 2017), with RE label providing a sharp boundary between MEC and parasubiculum (Varga et al., 2010; Witter et al., 2017) (see arrows in Figures 2A and 2E inset). We therefore performed immunohistochemical analysis comparing

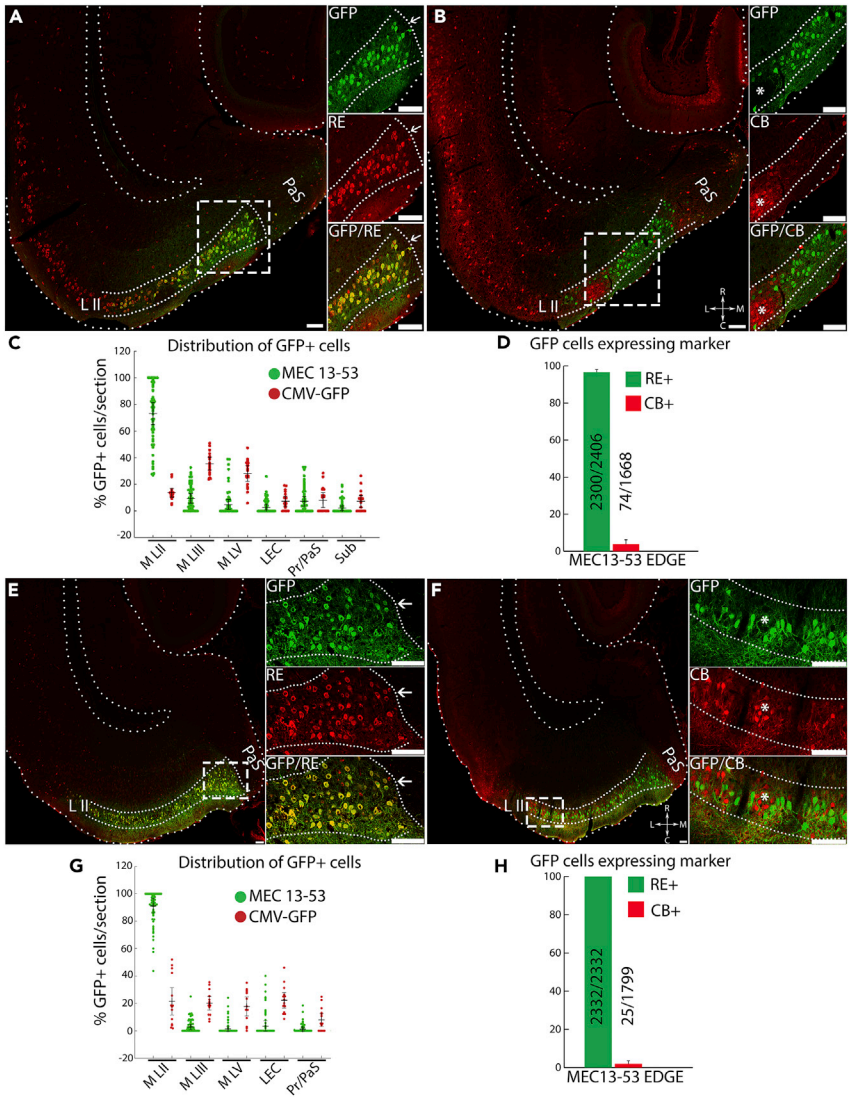

Figure 2. MEC13-53 EDGE rAAVs Recapitulates the Cell-Type Specificity Seen in the MEC13-53 EDGE Transgenic Crosses in WT Mice and Rats

Equal amount of MEC13-53 rAAV was injected into MEC of wild-type mice (A–D) and rats (E–H). Insets show anti-GFP (top), marker (middle), and overlay (bottom) of box in main panel. Sections of MEC13-53 rAAV injections counterstained with anti-RE antibody (red, [A] and [E]) and anti-CB antibody (red, [B] and [F]); with a CB + cluster (asterisks) in the insets in (B) and (F). Note the extensive co-localization of the RE stain with the GFP, the sharp delineation of the entorhinal/parasubicular boundary by both labels (arrows, [A] and [E]), and the exclusion of viral label from the CB clusters (asterisks, [B] and [F]).

(C) Proportion of GFP-expressing cells in different parahippocampal regions for both MEC13-53 and nonspecific CMV-rAAV. Each point is a section, note the large number of sections where 100% of the cells are in LII and 0% in other regions exclusively in the MEC13-53 rAAVs compared with the controls (for pictures of control injections see Figures 1B, S4, and S5). A total of 13,096 and 8,540 GFP + cells were counted from three mice injected with CMV-rAAV and seven mice with MEC13-53 rAAV, respectively; data represented as mean ± SEM. In (G), 7,191 and 2,831 GFP + cells from sections were counted from MEC13-53 rAAV and CMV-rAAV, respectively, from three rats. Quantitation of results are shown in (D) (for mice) and (H) (for rats), showing overlap of GFP with cell-marker Reelin stain (green) in LII MEC of mice (96%) and rats (complete overlap). About 4% overlap of GFP with Calbindin (red) was observed in mice and <2% overlap in rats, with number of cells counted in MECLII region. MEC-LII GFP + cells were counted from separate RE and CB immunostained sections from seven mice and three rats injected with MEC13-53 rAAV; data represented as mean ± SEM. See also related Figures S3–S6. Scale bar, 100 μm; all images were processed identically.

these markers with viral GFP and found that, for the MEC13-53 rAAV, 96% (2,300/2,406) of GFP + cells in layer II were RE+ (Figures 2A and 2D), whereas 4% (74/1,668) were CB+ (Figures 2B and 2D). In contrast, for injections of roughly equal amounts of the ubiquitous CMV-rAAV, only 34% (319/929) of GFP + LII cells were RE +, whereas 10.5% (142/1,353) were CB+. Thus, the MEC13-53 rAAV drives transgene expression specifically in a particular subset of excitatory neurons in EC of wild-type mice, i.e., RE + EC LII neurons (stellate cells in MEC), avoiding the adjacent CB + pyramidal cells, like the transgenic lines based on the same enhancer.

Although this nicely illustrates the specificity of this EDGE rAAV, perhaps the greatest utility of EDGE rAAVs is that, because enhancers are highly conserved (Cotney et al., 2013) and can be obtained from any tissue sample, they have the potential to work across species. As seen in Figures 2E–2G, S3C, and S4C, the MEC13-53 rAAV derived from mouse EC is, if anything, *more* specific in the rat. Figures 2E and S3C shows GFP expression almost exclusively in MEC LII (as quantified in Figures 2G and S6B), whereas the few labeled neurons in the virus with no enhancer have no layer specificity (Figure S3D), just as in mouse (Figure S3B). Similarly, 100% (2,332/2,332) of MEC LII GFP + neurons in rats injected with MEC13-53 rAAVs were RE+ (Figures 2E and 2H), whereas only 1.4% (25/1,799) were CB+ (Figures 2F and 2H), even though the two excitatory subtypes are intermingled (Witter et al., 2017). This, and the presence of LII-specific label throughout the dorsoventral and medio-lateral axes of the MEC (Figure S4C), provides compelling evidence for cellular specificity. Note that, with the nonspecific CMV-rAAV, 35% (189/518) of GFP + LII cells were RE +, whereas 46% (285/613) were CB+ (Figure S5). It is interesting to note that, although these two markers are largely mutually exclusive, there are reports of a very small subpopulation of RE + neurons that are also CB+ (Fuchs et al., 2016; Varga et al., 2010), so the single-digits label with the MEC13-53 virus may be those cells. Clearly, though, the two rAAVs with the same serotype have very different expression patterns, both in terms of layer and cellular specificity.

Systemic Administration of Blood-Brain Barrier Crossing MEC13-53 EDGE Recapitulates MEC Layer II Stellate Cell Expression

Although we are mainly interested in developing tools to be used in analysis of the EC, it is interesting to ask whether this enhancer would express in other brain regions if it were systemically administered. We therefore packaged the MEC13-53 EDGE enhancer (shown with the 2/1 serotype in Figures 1 and 2) into the blood-brain barrier crossing PHP (Deverman et al., 2016) serotype and performed noninvasive intravenous injections via the tail vein. Systemic injections of MEC13-53 EDGE PHP resulted in much sparser GFP + cells overall, but they are also mostly confined to layer II of MEC throughout the caudal forebrain (Figures 3A and S7). However, we also noticed sparse expression of the transgene in regions other than MEC, typically also in brain regions we would sometimes see transgene expression in MEC13-53 transgenic lines (Figures 3B and 3C, Table S2). Curiously, we did not see expression in LII of the piriform cortex, the major site of non-EC expression in the MEC13-53 transgenic lines, possibly due to the particular tropism of the PHP capsid. Furthermore, we confirmed that these GFP + cells in MEC are RE+ (Figure 3D). These results suggest that EDGE rAAV can retain its particular cell-type specificity, even when assembled in a serotype with a different innate tropism.

EDGE rAAVs Recapitulate the Expression Pattern of Their Respective Transgenic Lines

To examine whether this is a general strategy, we created EDGE rAAVs with several other enhancers with known specificity (Blankvoort et al., 2018). Although not all enhancers that worked as transgenic lines worked in rAAVs, roughly half (Figure 4, left column) did indeed appear to recapitulate the specificity (or relative lack thereof, 4A, B) of the corresponding EDGE lines (Figure 4, right column). The MEC13-104 rAAV (Figure 4A) recapitulates the relatively sparse labeling of a subset of LIII neurons (arrows) seen in the MEC13-104 line (Figure 4B), whereas the converse is true for the mainly LIII-specific LEC13-8 (compare 4C with 4D) line. Thus, the relative densities of the layer-specific label appear to be enhancer specific, suggesting that the minority of cells that strongly express outside of their primary layer may not be "noise." Ongoing experiments explore the functional distinctions between the cells labeled by the various enhancers, which may label distinct subsets of what has been considered a single neuronal cell type, e.g., stellate cells.

DISCUSSION

Our prior work showed that identification of cis-regulatory elements uniquely active in finely dissected cortical subregions allows one to generate genetic tools specific to cells in that subregion, an approach

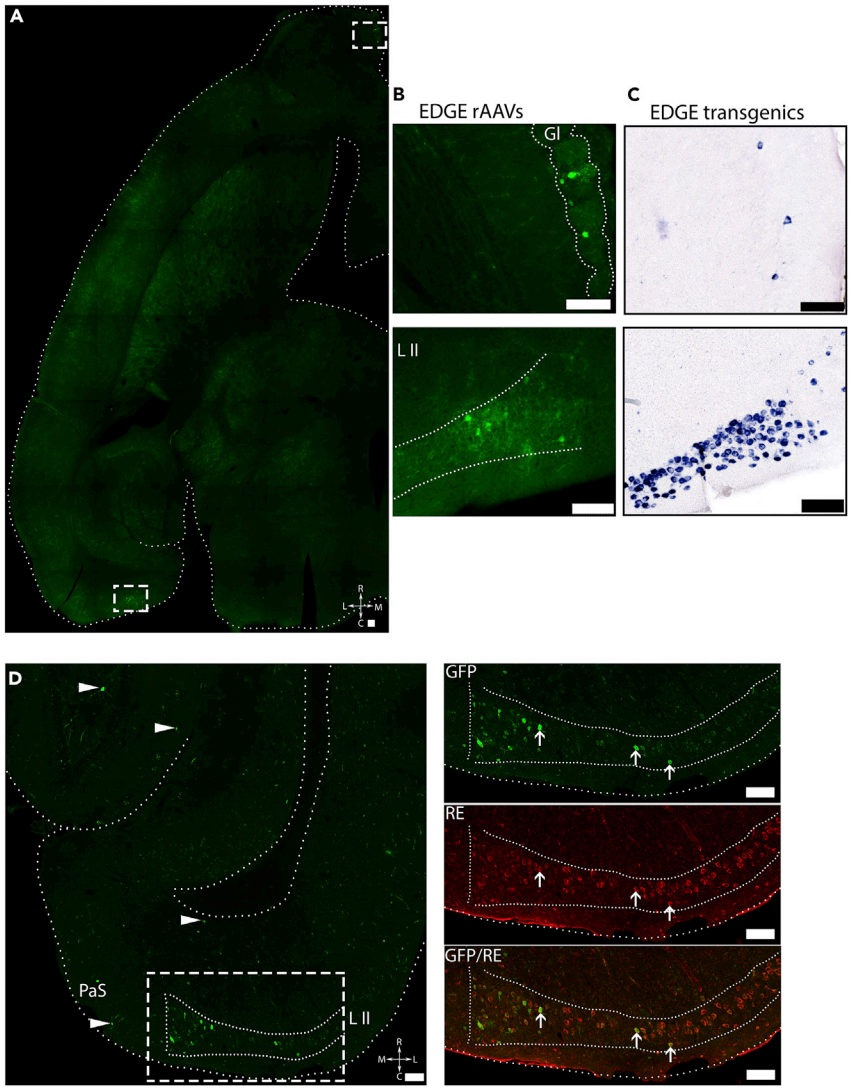

Figure 3. Recapitulation of LII MEC Specificity of MEC13-53 Using a BBB-Crossing rAAV Serotype

(A and B) (A) Representative image of the GFP + neurons in horizontal brain section from a mouse injected with 10^{12} particles of MEC13-53 rAAV PHP, intravenously into tail vein. The boxes in (A) are zoomed in (B).

(C) MEC13-53 transgene expression in same regions as in (B) are in the MEC13-53 tTA X tetO-TVAG transgenic cross.

(D) Sections of MEC13-53 rAAV PHP injected brain counterstained with anti-RE antibody. Insets show anti-GFP (top), Reelin (middle), and overlay (bottom) of box in main panel. Label is throughout the layers of EC and sparsely in other regions (arrow heads, [D]). Note the extensive co-localization of the RE stain with the GFP (arrows).

See also Figure S7. Scale bar, 100 μm. See also related Table S2.

we call EDGE (Blankvoort et al., 2018). Here we show that one can use the same approach to make rAAVs with similar specificity in both mouse and rat, provided the vector and minimal promoter's innate transcriptional activity is minimized. This clearly cross-validates the initial identification of enhancers in our prior work (Blankvoort et al., 2018): although transgenic lines might show highly specific expression patterns purely due to insertional effects (although *not* the same pattern in multiple founders, as we saw), rAAVs typically do not insert into the genome (Mccarty et al., 2004), so cannot show such effects. In other words, although the precise functional significance of the enhancers presented here remains unknown, they clearly are "true" enhancers, reflecting some genetic subgroup of excitatory neurons in the entorhinal cortex of wild-type mice and rats. Taken together, these data lead to two very interesting conclusions: (1) given that the numbers of enhancers may run into the millions (as opposed to ~44,000 promoters) (ENCODE Project Consortium, 2012), they may provide access to the ever-growing number of neuronal cell types

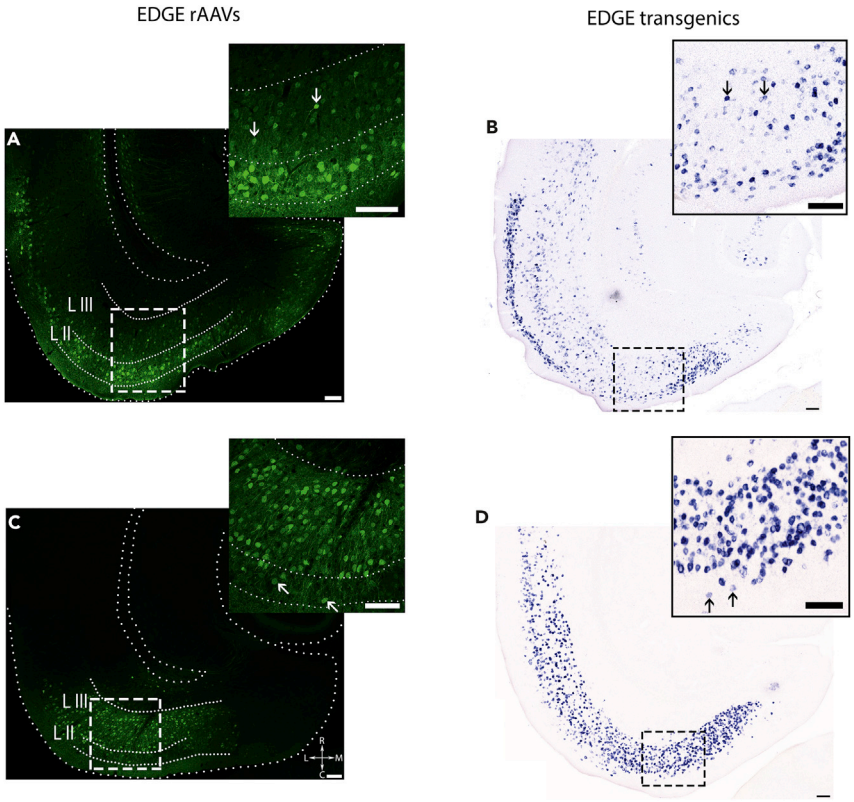

Figure 4. EDGE rAAVs Recapitulate the Distinct Layer-Specific Expression Patterns Seen in EDGE Transgenic Mice

Comparison of expression patterns obtained by injection of EDGE rAAVs (left column) with those seen in transgenic crosses made with the same enhancers (right column). Wild-type mice were injected with 400 nL of EDGE rAAVs (A) MEC13-104 and (C) LEC13-8. Transgene expression in the corresponding EDGE transgenic crosses ([B], MEC13-104 tTA X tetO-TVAG) and ([D], LEC13-8 tTA X tetO-HM3) visualized by ISH on horizontal sections using the respective transgene probes. The sparse expression of the transgene in minor layers is indicated by arrows both in EDGE transgenics and viruses. Scale bar, 100 μm; all sections are horizontal, and all rAAV figures underwent the same image processing. See also related Table S1 and Data S1.

than promoters, which may be far greater than generally assumed (Zeisel et al., 2015; Cembrowski et al., 2016; Tasic et al., 2018; Saunders et al., 2018); and (2) although we do not do so here, one could conceivably take this approach toward generating neuronal subtype-specific transgene expression in species other than the traditional genetic models of mouse, zebrafish, fly, and worm, because one can do the required epigenomic analyses on any tissue sample.

There has been a lot of effort over the years toward making cell-type-specific viral vectors, but even in those cases when a minimal native promoter is useful (i.e., when a single marker defines the cells, e.g., TH-AAV [Gompf et al., 2015] and CaMKII-AAV [Nathanson et al., 2009]) the AAVs are not fully restricted to cells expressing the gene. We have previously shown that using single, uniquely active enhancers can lead to far greater specificity than that of native parent promoters (Blankvoort et al., 2018), at least in transgenesis. That enhancers drive expression similarly in both transgenic lines and viruses is not a particularly surprising result. It has been known for decades that enhancers drive cell-specific expression (Grosveld et al., 1987; Noonan and Mccallion, 2010; Shen et al., 2016) in a variety of species. Enhancers for the six homeobox genes related to the fly *distal-less* gene (Cohen and Jurgens, 1989) (*Dll* in fly, Dlx in vertebrates) have been shown to play a crucial role in morphogenesis in many species (Anderson et al., 1997; Ghanem et al., 2003; Miyoshi et al., 2010; Panganiban and Rubenstein, 2002; Zerucha et al., 2000). One such enhancer in the Dlx 5/6 gene cluster has been shown to be critical to the development of interneurons in particular (Stenman et al., 2003), and a recent paper (Dimidschstein et al., 2016) used this enhancer element in a viral vector to obtain interneuron-specific expression in a variety of species, nicely showing

that enhancers can be used to drive expression in viral vectors. However, as is true for most genetically defined enhancers active early in development, Dlx5/6 drives expression across broad classes of neurons (e.g., interneurons in general) throughout the brain, rather than to particular interneuronal subclasses and/or subregions.

More recently, several groups have begun to incorporate cis-regulatory elements into their strategies for creating viral vectors specific to neuronal subtypes. Such efforts are likely furthest along in the retina, where Juttner and colleagues (2019) created a broad rAAV resource targeting subtypes of retinal neurons using strategies based on genes of interest (GOIs) identified in *a priori* transcriptomal analysis (Siegert et al., 2012) and epigenetic analysis (Hartl et al., 2017) of known retinal cell types. Although most of these constructs are simply the minimal promoters of the GOIs, some also are based on the local epigenetic landscape, using strategies such as conservation, methylation patterns, and transcription factor binding sites to identify likely *cis*-elements for GOIs. Although the results in retina can be quite impressive, little is known how specific such vectors would be in the rest of the brain. As for the brain, Hrvatin et al., 2019 recently published an interesting screening strategy called PESCA (Paralleled Enhancer Single Cell Assay), in which multiple rAAVs containing barcoded putative enhancers (they use the term Gene Regulatory Elements, or GREs) are screened via single-cell transcriptomics (scRNAseq) rather than the more traditional one-at-a-time anatomical techniques shown here. Although scRNAseq does not always reflect actual viral expression, this technique nevertheless promises to greatly increase the throughput involved in first-pass screening of rAAVs. In a very interesting study, Graybuck and colleagues compare scRNAseq data to the epigenetic single-cell Assay for Transposase-Accessible Chromatin with Sequencing (scATACseq) data from layer-specific transgenic mice. Hits that co-register in both the transcriptomic and epigenetic clusters are then cloned into PHP.B Cre-rAAVs and systemically (retro-orbitally) injected into a Cre-reporter mouse for anatomical characterization.

The overwhelming similarity of these various approaches is the idea that individual *cis*-regulatory elements may be more specific than promoters. Each strategy has two stages: **identifying** likely *cis*-regulatory elements and then making and **screening** the resulting rAAVs. The major difference clearly comes at the identification stage: each of these other GRE (as opposed to promoter) -based approaches has been based on *a priori* knowledge of the transcriptomics of whatever cell type one is looking for, often even taking advantage of transgenic animals, whereas EDGE simply looks for regionally specific chromatin marks in reproducibly dissected bulk tissue. The advantage of the former is resolution: by a "deep dive" into subtypes of what we had originally thought *were* cell types, one both gets at the scale of neuronal diversity and immediately puts the cell types in context, whereas with pure differential screens of bulk tissue such as EDGE you really do not know what cell types you will get, you just know that they are more or less specific to your tissue of interest. However, the flexibility (one simply needs ChIP of an ROI), ease of doing EDGE in other species, and ability to discover truly new cell types counterbalance this disadvantage. A more purely technical difference is between bulk ChIPseq and ATACseq. Although the latter can be done with much less tissue (even single cells), the former's use of particular histone marks may provide greater specificity for active enhancers rather than other forms of open chromatin. At the screening level, systemic viral injections (Graybuck, 2019) with AAV serotypes that cross the blood-brain barrier clearly give you the best idea of where a particular enhancer can express throughout the brain. We regret that we are as of yet unable to obtain permission to perform retro-orbital AAV injections from our local regulators, so our systemic injections were with a less effective technique (tail vein), lowering the effective titer. If PESCA (Hrvatin et al., 2019) can reliably be done on bulk tissue, however, it may end up as a better screen for our purposes. All in all, there are advantages to each approach that make them largely complementary, suggesting that combinations of these techniques and comparisons between the resulting datasets (ChIP versus ATAC, bulk versus single cell) may well end up being the best overall approach.

Thus, the most important aspect of these and other papers is not that enhancers can work in viral vectors, it is illustrating the promise of applying modern genomic techniques to the study of the precise neural circuitry of the vertebrate brain. The striking diversity of enhancers found in these tiny subregions of cortex (numbers comparable with those found for entire organs) may indicate a similar diversity of neuronal cell types in the brain. However, the relationship between enhancers and cell types remains unclear. Indeed, the expression patterns we obtain are arguably more specific than our current understanding of neuronal cell type (Luo et al., 2008; Zeng and Sanes, 2017). For instance, stellate cells are a generally accepted excitatory neuronal cell type of the medial entorhinal cortex (Rowland et al., 2016; Varga et al., 2010; Witter et al.,

2017). However, we show that distinct enhancers drive expression in EC LII stellate cells to different degrees in both transgenics and rAAVs. The question becomes whether these enhancer-driven expression patterns reflect functionally distinct stellate cells, or states of stellate cells, or just random subsets of the same indivisible cell type. In the specific case of stellate cells, a recent paper used optogenetic tagging to show that stellate cells of the MEC exhibit a variety of quite distinct receptive field properties (i.e., they can be grid cells or spatial cells or border cells), suggesting that there are many functional subtypes of stellate cells (Rowland et al., 2018). More generally, the relationship between differential enhancer usage and neuronal cell types is a highly non-trivial question, not least because there is not even complete agreement even as to *how* to define neuronal cell types (although there are notable exceptions) (Cembrowski et al., 2016; Tasic et al., 2018; Tremblay et al., 2016), let alone how many there are. There are several other interesting explanations for differential enhancer usage beyond cell type; for instance, it could dictate distinct states of a single cell type. In support of this, neural activity drastically changes the chromatin landscape of the brain, including which enhancers are active (Gallegos et al., 2018; Malik et al., 2014). It will likely take years of anatomical, molecular, and physiological characterization of these tools to disentangle such questions, so for our current purposes the most important consideration is that these enhancer-based molecular genetic tools remain true to type, as appears to largely be the case, comparing the virus to the transgenic.

It should be noted, however, that specificity is almost never absolute, especially with viral vectors. Although we obtain neuronal subtype-specific results with large injections into the entorhinal cortex (Figures 2 and S4), it is likely that any cell type in other brain regions that express the transcription factor(s) appropriate for a particular enhancer would be labeled as well, as can be seen with the systemic injections shown in Figure 3. Thus, we do not claim that the rAAVs shown here are necessarily 100% regionally specific; indeed, it is hard to imagine that a particular enhancer is only used once in development. Rather, we demonstrate clear cell-type specificity when the MEC13-53 rAAV is injected into a particular brain region, which is nevertheless good enough for the study of neural circuitry. Moreover, many more cells are infected than show strong GFP label, and there is a baseline level of transcription from other elements in the viral construct (i.e., the minimal promoter and the ITRs). This implies that superfection of enough rAAVs could lead to discernible nonspecific transgene expression in any cell regardless of the promoter, something that is shown most clearly by making viruses containing no exogenous promoter whatsoever (Figure 1C). Viral expression is thus not all-or-nothing, but the difference between background and enhancer-driven expression levels can be quite marked (Figure S1). This background expression inherent to rAAVs can be quite problematic when a little bit of expression can have a large effect. This is true when expressing enzymes such as recombinases or when complementing replication-competent viruses (e.g., pseudotyped ΔG-rabies [Weible et al., 2010]) but is likely not an issue with transgenes whose effects vary roughly linearly with their expression levels, such as the chemogenetic (Sternson and Roth, 2014) and/or optogenetic tools (Boyden et al., 2005) used to study neural circuits.

Thus, identification of the active enhancers of a mere four cortical subregions of the mouse brain has led to a variety of transgenic, and now viral tools for circuit analysis that appear to work across species, at least in rodents. Since, in principle, one can do this on any reasonably well-annotated genome, one could conceivably develop tools for anatomically specific "circuit-breaking" tools in *any* species, even our own. Thus, not only will circuit-specific tools greatly facilitate our understanding of normal and pathological brain function, but they could also in time possibly provide circuit-specific therapeutic avenues. For example, it has been known for decades that preclinical stages of Alzheimer's disease (AD) are characterized by neuronal loss and accumulation of neurofibrillary tangles in the superficial layers of trans-entorhinal cortex (Braak and Braak, 1991), a region roughly equivalent to rodent MEC layer II. In addition, intracellular amyloid-β is found specifically in MEC layer II RE + neurons in human AD pathology and rodent disease models (Kobro-Flatmoen et al., 2016). Given the emerging consensus that AD may progress trans-synaptically (De Calignon et al., 2012; Spires-Jones and Hyman, 2014), it is conceivable that one could use something like a MEC13-53 rAAV to deliver therapeutic agents directly to the presumed pre-α cells, thereby stopping AD before it starts. More generally, it is possible that the reason that many neurological and neuropsychiatric disorders are resistant to drug therapy is that they are imbalances in particular neural circuits, not diseases of the entire brain. A drug having tropism for multiple circuits (as most do) would then by definition produce unwanted side effects: it may do the right thing in the right circuit, but it does the wrong thing to normal circuits. Results like those presented here allow the hope that investigators may one day be able to design interventions with the specificity required to treat the complex diseases of the brain.

Limitations of the Study

Although we think that we have made a substantive contribution toward the generation of circuit-specific tools that could be used outside of traditional genetic models, we freely acknowledge the limitations of our data. Although it is indeed true that active enhancers can be identified in any tissue sample of reasonable size from any species and used to make EDGE-rAAVs in ways similar to that presented here, we have only showed the same specificity for stellate cells in two rodent species—larger animals such as primates pose significant challenges with viral vectors. In addition, although we can see remarkable cellular specificity when EDGE rAAVs are injected into the region they were designed for, systemic administration suggests that the enhancer may also express in other cell types if injected in other regions. Regardless, we feel that these are quite useful tools for the analysis of neural circuits.

METHODS

All methods can be found in the accompanying Transparent Methods supplemental file.

SUPPLEMENTAL INFORMATION

Supplemental Information can be found online at https://doi.org/10.1016/j.isci.2020.100888.

ACKNOWLEDGMENTS

The work was funded by FRIPRO ToppForsk grant Enhanced Transgenics (90096000) of the Research Council of Norway, the Kavli Foundation, the Center of Excellence scheme of the Research Council of Norway-Centre for Biology of Memory and Centre for Neural Computation, The Egil and Pauline Braathen and Fred Kavli Centre for Cortical Microcircuits, and the National Infrastructure scheme of the Research Council of Norway-NORBRAIN. We acknowledge the help from Christina Schrick and Qiangwei Zhang for immunostainings and *in situ* hybridizations; Grethe M. Olsen and Miguel Carvalho for training on rat injections; Nicola P. Montaldo for demonstrating qPCR; Hanne M. Møllergård, Siv Eggen, and technicians at the animal facility (Kavli institute/CNC); May-Britt Moser, Ben Kanter, and Christine M. Lykken for valuable suggestions on the manuscript; and Tomas Bjorklund, Menno P. Witter, and members of Kentros lab for helpful discussions.

AUTHOR CONTRIBUTIONS

C.K., R.R.N., and S.B. conceptualized the study. R.R.N did the data curation. Formal analyses were done by R.R.N., M.J.L., and S.B. C.K. did the funding acquisition. Investigation was done by R.R.N., M.J.L., and S.B. Methodology was by R.R.N., S.B., and C.K. Project administration and supervision were done by C.K. and R.R.N. Resources for the study were from R.R.N., M.J.L., and S.B. Validation was by R.R.N., S.B., M.J.L., and C.K. Original draft was prepared by R.R.N. and C.K. Review and editing was by C.K., R.R.N., S.B., and M.J.L.

DECLARATION OF INTERESTS

C.K., S.B., and R.R.N. are inventors on US Patent Application no. 62/584,282, Appl. Norwegian University of Science and Technology (NTNU), which is related to this work. The authors have no other competing interests to declare.

Received: July 8, 2019
Revised: December 3, 2019
Accepted: February 3, 2020
Published: March 27, 2020

REFERENCES

Anderson, S.A., Eisenstat, D.D., Shi, L., and Rubenstein, J.L. (1997). Interneuron migration from basal forebrain to neocortex: dependence on Dlx genes. Science *278*, 474–476.

Aschauer, D.F., Kreuz, S., and Rumpel, S. (2013). Analysis of transduction efficiency, tropism and axonal transport of AAV serotypes 1, 2, 5, 6, 8 and 9 in the mouse brain. PLoS One *8*, e76310.

Blankvoort, S., Witter, M.P., Noonan, J., Cotney, J., and Kentros, C. (2018). Marked diversity of unique cortical enhancers enables neuron-specific tools by enhancer-driven gene expression. Curr. Biol. *28*, 2103–2114.e5.

Boccara, C.N., Kjonigsen, L.J., Hammer, I.M., Bjaalie, J.G., Leergaard, T.B., and Witter, M.P. (2015). A three-plane architectonic atlas of the rat hippocampal region. Hippocampus *25*, 838–857.

Bouard, D., Alazard-Dany, D., and Cosset, F.L. (2009). Viral vectors: from virology to transgene expression. Br. J. Pharmacol. *157*, 153–165.

Boyden, E.S., Zhang, F., Bamberg, E., Nagel, G., and Deisseroth, K. (2005). Millisecond-timescale, genetically targeted optical control of neural activity. Nat. Neurosci. *8*, 1263–1268.

Braak, H., and Braak, E. (1991). Neuropathological stageing of Alzheimer-related changes. Acta Neuropathol. *82*, 239–259.

Callaway, E.M., and Luo, L. (2015). Monosynaptic circuit tracing with glycoprotein-deleted rabies viruses. J. Neurosci. *35*, 8979–8985.

Carter, B.J., Flotte, T., Afione, S. and Solow, R. 1993. Adeno-associated virus with inverted terminal repeat sequences as promoter. Google Patents.

Castle, M.J., Turunen, H.T., Vandenberghe, L.H., and Wolfe, J.H. (2016). Controlling AAV tropism in the nervous system with natural and engineered capsids. Methods Mol. Biol. *1382*, 133–149.

Cembrowski, M.S., Bachman, J.L., Wang, L., Sugino, K., Shields, B.C., and Spruston, N. (2016). Spatial gene-expression gradients underlie prominent heterogeneity of CA1 pyramidal neurons. Neuron *89*, 351–368.

Chen, T.-W., Wardill, T.J., Sun, Y., Pulver, S.R., Renninger, S.L., Baohan, A., Schreiter, E.R., Kerr, R.A., Orger, M.B., Jayaraman, V., et al. (2013). Ultra-sensitive fluorescent proteins for imaging neuronal activity. Nature *499*, 295–300.

Cohen, S.M., and Jurgens, G. (1989). Proximal-distal pattern formation in Drosophila: cell autonomous requirement for Distal-less gene activity in limb development. EMBO J. *8*, 2045–2055.

ENCODE Project Consortium (2012). An integrated encyclopedia of DNA elements in the human genome. Nature *489*, 57–74.

Cotney, J., Leng, J., Yin, J., Reilly, S.K., Demare, L.E., Emera, D., Ayoub, A.E., Rakic, P., and Noonan, J.P. (2013). The evolution of lineage-specific regulatory activities in the human embryonic limb. Cell *154*, 185–196.

Davidson, B.L., Stein, C.S., Heth, J.A., Martins, I., Kotin, R.M., Derksen, T.A., Zabner, J., Ghodsi, A., and Chiorini, J.A. (2000). Recombinant adeno-associated virus type 2, 4, and 5 vectors: transduction of variant cell types and regions in the mammalian central nervous system. Proc. Natl. Acad. Sci. U S A *97*, 3428–3432.

De Calignon, A., Polydoro, M., Suarez-Calvet, M., William, C., Adamowicz, D.H., Kopeikina, K.J., Pitstick, R., Sahara, N., Ashe, K.H., Carlson, G.A., et al. (2012). Propagation of tau pathology in a model of early Alzheimer's disease. Neuron *73*, 685–697.

Delzor, A., Dufour, N., Petit, F., Guillermier, M., Houitte, D., Auregan, G., Brouillet, E., Hantraye, P., and Deglon, N. (2012). Restricted transgene expression in the brain with cell-type specific neuronal promoters. Hum. Gene Ther. Methods *23*, 242–254.

Deverman, B.E., Pravdo, P.L., Simpson, B.P., Kumar, S.R., Chan, K.Y., Banerjee, A., Wu, W.L., Yang, B., Huber, N., Pasca, S.P., et al. (2016). Cre-dependent selection yields AAV variants for widespread gene transfer to the adult brain. Nat. Biotechnol. *34*, 204–209.

Dias, M.F., Joo, K., Kemp, J.A., Fialho, S.L., da Silva Cunha, A., Jr., Woo, S.J., and Kwon, Y.J. (2018). Molecular genetics and emerging therapies for retinitis pigmentosa: basic research and clinical perspectives. Prog. Retin. Eye Res. *63*, 107–131.

Dimidschstein, J., Chen, Q., Tremblay, R., Rogers, S.L., Saldi, G.A., Guo, L., Xu, Q., Liu, R., Lu, C., Chu, J., et al. (2016). A viral strategy for targeting and manipulating interneurons across vertebrate species. Nat. Neurosci. *19*, 1743–1749.

During, M.J., Young, D., Baer, K., Lawlor, P., and Klugmann, M. (2003). Development and optimization of adeno-associated virus vector transfer into the central nervous system. Methods Mol. Med. *76*, 221–236.

Feng, G., Mellor, R.H., Bernstein, M., Keller-Peck, C., Nguyen, Q.T., Wallace, M., Nerbonne, J.M., Lichtman, J.W., and Sanes, J.R. (2000). Imaging neuronal subsets in transgenic mice expressing multiple spectral variants of GFP. Neuron *28*, 41–51.

Flotte, T.R., Afione, S.A., Solow, R., Drumm, M.L., Markakis, D., Guggino, W.B., Zeitlin, P.L., and Carter, B.J. (1993). Expression of the cystic fibrosis transmembrane conductance regulator from a novel adeno-associated virus promoter. J. Biol. Chem. *268*, 3781–3790.

Fuchs, E.C., Neitz, A., Pinna, R., Melzer, S., Caputi, A., and Monyer, H. (2016). Local and distant input controlling excitation in layer II of the medial entorhinal cortex. Neuron *89*, 194–208.

Gallegos, D.A., Chan, U., Chen, L.F., and West, A.E. (2018). Chromatin regulation of neuronal maturation and plasticity. Trends Neurosci. *41*, 311–324.

Ghanem, N., Jarinova, O., Amores, A., Long, Q., Hatch, G., Park, B.K., Rubenstein, J.L., and Ekker, M. (2003). Regulatory roles of conserved intergenic domains in vertebrate Dlx bigene clusters. Genome Res. *13*, 533–543.

Gompf, H.S., Budygin, E.A., Fuller, P.M., and Bass, C.E. (2015). Targeted genetic manipulations of neuronal subtypes using promoter-specific combinatorial AAVs in wild-type animals. Front. Behav. Neurosci. *9*, 152.

Graybuck, L.T. (2019). Prospective, brain-wide labeling of neuronal subclasses with enhancer-driven AAVs. BioRxiv. https://doi.org/10.1101/525014.

Grosveld, F., van Assendelft, G.B., Greaves, D.R., and Kollias, G. (1987). Position-independent, high-level expression of the human beta-globin gene in transgenic mice. Cell *51*, 975–985.

Haberman, R.P., Mccown, T.J., and Samulski, R.J. (2000). Novel transcriptional regulatory signals in the adeno-associated virus terminal repeat A/D junction element. J. Virol. *74*, 8732–8739.

Hartl, D., Krebs, A.R., Juttner, J., Roska, B., and Schubeler, D. (2017). Cis-regulatory landscapes of four cell types of the retina. Nucleic Acids Res. *45*, 11607–11621.

Hauck, B., Chen, L., and Xiao, W. (2003). Generation and characterization of chimeric recombinant AAV vectors. Mol. Ther. *7*, 419–425.

Hrvatin, S., Tzeng, C.P., Nagy, M.A., Stroud, H., Koutsioumpa, C., Wilcox, O.F., Assad, E.G., Green, J., Harvey, C.D., Griffith, E.C., et al. (2019). A scalable platform for the development of cell-type-specific viral drivers. Elife *8*, https://doi.org/10.7554/eLife.48089.001.

Hutson, T.H., Verhaagen, J., Yanez-Munoz, R.J., and Moon, L.D. (2012). Corticospinal tract transduction: a comparison of seven adeno-associated viral vector serotypes and a non-integrating lentiviral vector. Gene Ther. *19*, 49–60.

Kanter, B.R., Lykken, C.M., Avesar, D., Weible, A., Dickinson, J., Dunn, B., Borgesius, N.Z., Roudi, Y., and Kentros, C.G. (2017). A novel mechanism for the grid-to-place cell transformation revealed by transgenic depolarization of medial entorhinal cortex layer II. Neuron *93*, 1480–1492.e6.

Kitamura, T., Pignatelli, M., Suh, J., Kohara, K., Yoshiki, A., Abe, K., and Tonegawa, S. (2014). Island cells control temporal association memory. Science *343*, 896–901.

Klimczak, R.R., Koerber, J.T., Dalkara, D., Flannery, J.G., and Schaffer, D.V. (2009). A novel adeno-associated viral variant for efficient and selective intravitreal transduction of rat Muller cells. PLoS One *4*, e7467.

Kobro-Flatmoen, A., Nagelhus, A., and Witter, M.P. (2016). Reelin-immunoreactive neurons in entorhinal cortex layer II selectively express intracellular amyloid in early Alzheimer's disease. Neurobiol. Dis. *93*, 172–183.

Koerber, J.T., Jang, J.H., and Schaffer, D.V. (2008). DNA shuffling of adeno-associated virus yields functionally diverse viral progeny. Mol. Ther. *16*, 1703–1709.

Koerber, J.T., Klimczak, R., Jang, J.H., Dalkara, D., Flannery, J.G., and Schaffer, D.V. (2009). Molecular evolution of adeno-associated virus for enhanced glial gene delivery. Mol. Ther. *17*, 2088–2095.

Kotterman, M.A., and Schaffer, D.V. (2014). Engineering adeno-associated viruses for clinical gene therapy. Nat. Rev. Genet. *15*, 445–451.

Kugler, S., Kilic, E., and Bahr, M. (2003). Human synapsin 1 gene promoter confers highly neuron-specific long-term transgene expression from an adenoviral vector in the adult rat brain depending on the transduced area. Gene Ther. *10*, 337–347.

Loew, R., Heinz, N., Hampf, M., Bujard, H., and Gossen, M. (2010). Improved Tet-responsive promoters with minimized background expression. BMC Biotechnol. *10*, 81.

Luo, L., Callaway, E.M., and Svoboda, K. (2008). Genetic dissection of neural circuits. Neuron *57*, 634–660.

Malik, A.N., Vierbuchen, T., Hemberg, M., Rubin, A.A., Ling, E., Couch, C.H., Stroud, H., Spiegel, I., Farh, K.K., Harmin, D.A., et al. (2014). Genome-wide identification and characterization of functional neuronal activity-dependent enhancers. Nat. Neurosci. *17*, 1330–1339.

Matthaei, K.I. (2007). Genetically manipulated mice: a powerful tool with unsuspected caveats. J. Physiol. *582*, 481–488.

Mccarty, D.M., Young, S.M., Jr., and Samulski, R.J. (2004). Integration of adeno-associated virus (AAV) and recombinant AAV vectors. Annu. Rev. Genet. *38*, 819–845.

Mcclure, C., Cole, K.L., Wulff, P., Klugmann, M., and Murray, A.J. (2011). Production and titering of recombinant adeno-associated viral vectors. J. Vis. Exp. *57*, e3348.

Mendell, J.R., Al-Zaidy, S., Shell, R., Arnold, W.D., Rodino-Klapac, L.R., Prior, T.W., Lowes, L., Alfano, L., Berry, K., Church, K., et al. (2017). Single-dose gene-replacement therapy for spinal muscular atrophy. N. Engl. J. Med. *377*, 1713–1722.

Miao, C., Cao, Q., Moser, M.B., and Moser, E.I. (2017). Parvalbumin and somatostatin interneurons control different space-coding networks in the medial entorhinal cortex. Cell *171*, 507–521.e17.

Miyoshi, G., Hjerling-Leffler, J., Karayannis, T., Sousa, V.H., Butt, S.J., Battiste, J., Johnson, J.E., Machold, R.P., and Fishell, G. (2010). Genetic fate mapping reveals that the caudal ganglionic eminence produces a large and diverse population of superficial cortical interneurons. J. Neurosci. *30*, 1582–1594.

Nathanson, J.L., Yanagawa, Y., Obata, K., and Callaway, E.M. (2009). Preferential labeling of inhibitory and excitatory cortical neurons by endogenous tropism of adeno-associated virus and lentivirus vectors. Neuroscience *161*, 441–450.

Noonan, J.P., and Mccallion, A.S. (2010). Genomics of long-range regulatory elements. Annu. Rev. Genomics Hum. Genet. *11*, 1–23.

Panganiban, G., and Rubenstein, J.L. (2002). Developmental functions of the Distal-less/Dlx homeobox genes. Development *129*, 4371–4386.

Roth, B.L. (2016). DREADDs for neuroscientists. Neuron *89*, 683–694.

Rowland, D.C., Obenhaus, H.A., Skytoen, E.R., Zhang, Q., Kentros, C.G., Moser, E.I., and Moser, M.B. (2018). Functional properties of stellate cells in medial entorhinal cortex layer II. Elife *7*, https://doi.org/10.7554/eLife.36664.001.

Rowland, D.C., Roudi, Y., Moser, M.B., and Moser, E.I. (2016). Ten years of grid cells. Annu. Rev. Neurosci. *39*, 19–40.

Saunders, A., Macosko, E.Z., Wysoker, A., Goldman, M., Krienen, F.M., De Rivera, H., Bien, E., Baum, M., Bortolin, L., Wang, S., et al. (2018). Molecular diversity and specializations among the cells of the adult mouse brain. Cell *174*, 1015–1030.e16.

Shen, S.Q., Myers, C.A., Hughes, A.E., Byrne, L.C., Flannery, J.G., and Corbo, J.C. (2016). Massively parallel cis-regulatory analysis in the mammalian central nervous system. Genome Res. *26*, 238–255.

Shevtsova, Z., Malik, J.M., Michel, U., Bahr, M., and Kugler, S. (2005). Promoters and serotypes: targeting of adeno-associated virus vectors for gene transfer in the rat central nervous system in vitro and in vivo. Exp. Physiol. *90*, 53–59.

Siegert, S., Cabuy, E., Scherf, B.G., Kohler, H., Panda, S., Le, Y.Z., Fehling, H.J., Gaidatzis, D., Stadler, M.B., and Roska, B. (2012). Transcriptional code and disease map for adult retinal cell types. Nat. Neurosci. *15*, 487–495, S1-2.

Spires-Jones, T.L., and Hyman, B.T. (2014). The intersection of amyloid beta and tau at synapses in Alzheimer's disease. Neuron *82*, 756–771.

Stenman, J., Toresson, H., and Campbell, K. (2003). Identification of two distinct progenitor populations in the lateral ganglionic eminence: implications for striatal and olfactory bulb neurogenesis. J. Neurosci. *23*, 167–174.

Sternson, S.M., and Roth, B.L. (2014). Chemogenetic tools to interrogate brain functions. Annu. Rev. Neurosci. *37*, 387–407.

Tasic, B., Yao, Z., Graybuck, L.T., Smith, K.A., Nguyen, T.N., Bertagnolli, D., Goldy, J., Garren, E., Economo, M.N., Viswanathan, S., et al. (2018). Shared and distinct transcriptomic cell types across neocortical areas. Nature *563*, 72–78.

Tervo, D.G., Hwang, B.Y., Viswanathan, S., Gaj, T., Lavzin, M., Ritola, K.D., Lindo, S., Michael, S., Kuleshova, E., Ojala, D., et al. (2016). A designer AAV variant permits efficient retrograde Access to projection neurons. Neuron *92*, 372–382.

Tremblay, R., Lee, S., and Rudy, B. (2016). GABAergic interneurons in the neocortex: from cellular properties to circuits. Neuron *91*, 260–292.

Varga, C., Lee, S.Y., and Soltesz, I. (2010). Target-selective GABAergic control of entorhinal cortex output. Nat. Neurosci. *13*, 822–824.

Wang, C., Wang, C.M., Clark, K.R., and Sferra, T.J. (2003). Recombinant AAV serotype 1 transduction efficiency and tropism in the murine brain. Gene Ther. *10*, 1528–1534.

Watakabe, A., Ohtsuka, M., Kinoshita, M., Takaji, M., Isa, K., Mizukami, H., Ozawa, K., Isa, T., and Yamamori, T. (2015). Comparative analyses of adeno-associated viral vector serotypes 1, 2, 5, 8 and 9 in marmoset, mouse and macaque cerebral cortex. Neurosci. Res. *93*, 144–157.

Weible, A.P., Schwarcz, L., Wickersham, I.R., Deblander, L., Wu, H., Callaway, E.M., Seung, H.S., and Kentros, C.G. (2010). Transgenic targeting of recombinant rabies virus reveals monosynaptic connectivity of specific neurons. J. Neurosci. *30*, 16509–16513.

Witter, M.P., Doan, T.P., Jacobsen, B., Nilssen, E.S., and Ohara, S. (2017). Architecture of the entorhinal cortex A review of entorhinal anatomy in rodents with some comparative notes. Front. Syst. Neurosci. *11*, 46.

Zeisel, A., Munoz-Manchado, A.B., Codeluppi, S., Lonnerberg, P., La Manno, G., Jureus, A., Marques, S., Munguba, H., He, L., Betsholtz, C., et al. (2015). Brain structure. Cell types in the mouse cortex and hippocampus revealed by single-cell RNA-seq. Science *347*, 1138–1142.

Zeng, H., and Sanes, J.R. (2017). Neuronal cell-type classification: challenges, opportunities and the path forward. Nat. Rev. Neurosci. *18*, 530–546.

Zerucha, T., Stuhmer, T., Hatch, G., Park, B.K., Long, Q., Yu, G., Gambarotta, A., Schultz, J.R., Rubenstein, J.L., and Ekker, M. (2000). A highly conserved enhancer in the Dlx5/Dlx6 intergenic region is the site of cross-regulatory interactions between Dlx genes in the embryonic forebrain. J. Neurosci. *20*, 709–721.

Zufferey, R., Donello, J.E., Trono, D., and Hope, T.J. (1999). Woodchuck hepatitis virus posttranscriptional regulatory element enhances expression of transgenes delivered by retroviral vectors. J. Virol. *73*, 2886–2892.

iScience, Volume *23*

Supplemental Information

Enhancer-Driven Gene Expression (EDGE) Enables the Generation of Viral Vectors Specific to Neuronal Subtypes

Rajeevkumar Raveendran Nair, Stefan Blankvoort, Maria Jose Lagartos, and Cliff Kentros

Supplemental information

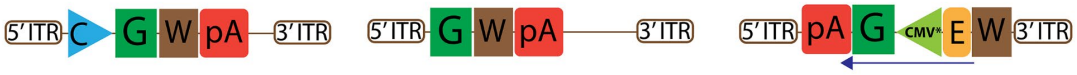

Image settings to visualize all in similar intensity

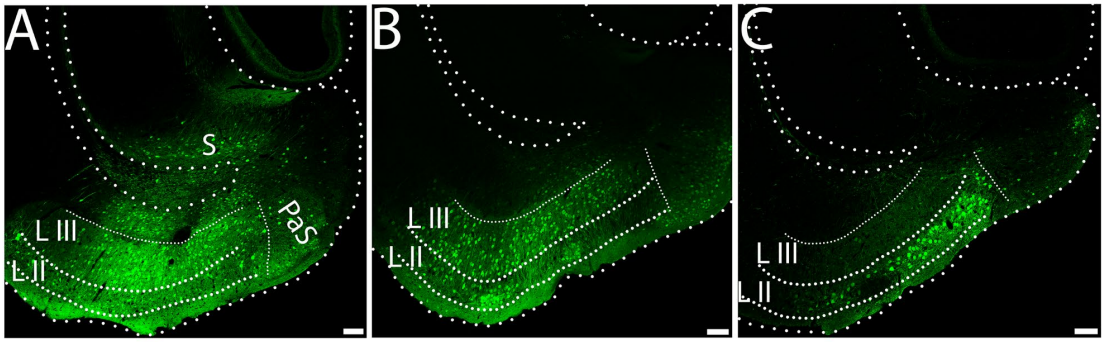

Image settings to visualize D

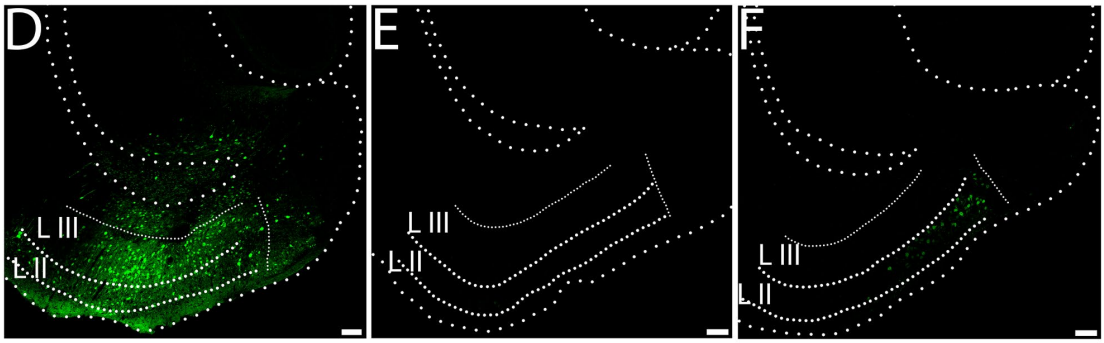

Image settings to visualize H

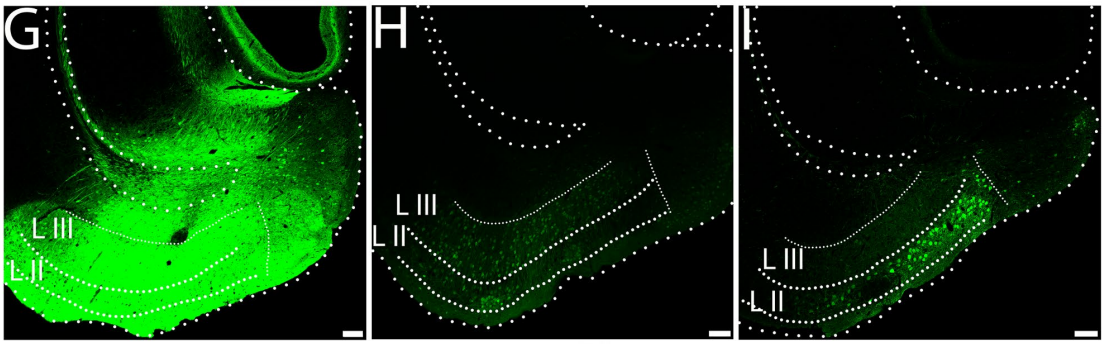

Image settings to visualize L

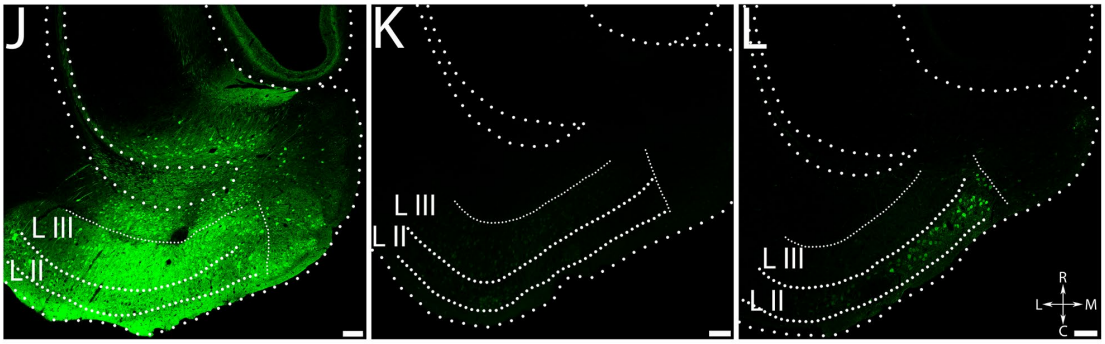

Figure S1. Visualization of GFP signal depends critically on post-processing (related to Figure 1). *The same images shown optimally in Figure 1B-D are shown with the same post-acquisition processing for the purposes of comparison of strong versus weak viral GFP expression seen with the different viral constructs. Left column is CMV rAAV, middle column is the promoterless-rAAV, and the right column is the MEC13-53 rAAV. Top row (S1A-C) shows images at optimized settings as shown in Figure 1B-D; second row (S1D-F) shows images at optimization settings for CMV-rAAV applied to all images; third row (S1G-I) shows optimization settings for promoterless-rAAV; fourth row (S1J-L) shows optimization settings for MEC13-53 rAAV. Note that at the settings for both CMV-rAAV and MEC13-53 the background GFP seen in the promoterless-rAAV (S1E, K) is not visible, while at the settings optimized for promoterless-rAAV the label in the parenchyma makes it impossible to visualize individual cells in the CMV-rAAV, and makes it look like there is (much lighter) label in LIII in the MEC13-53 rAAV (see Figure 1D inset). Schematics of the viral designs are depicted on top of the corresponding image. Scale bar = 100 μm.*

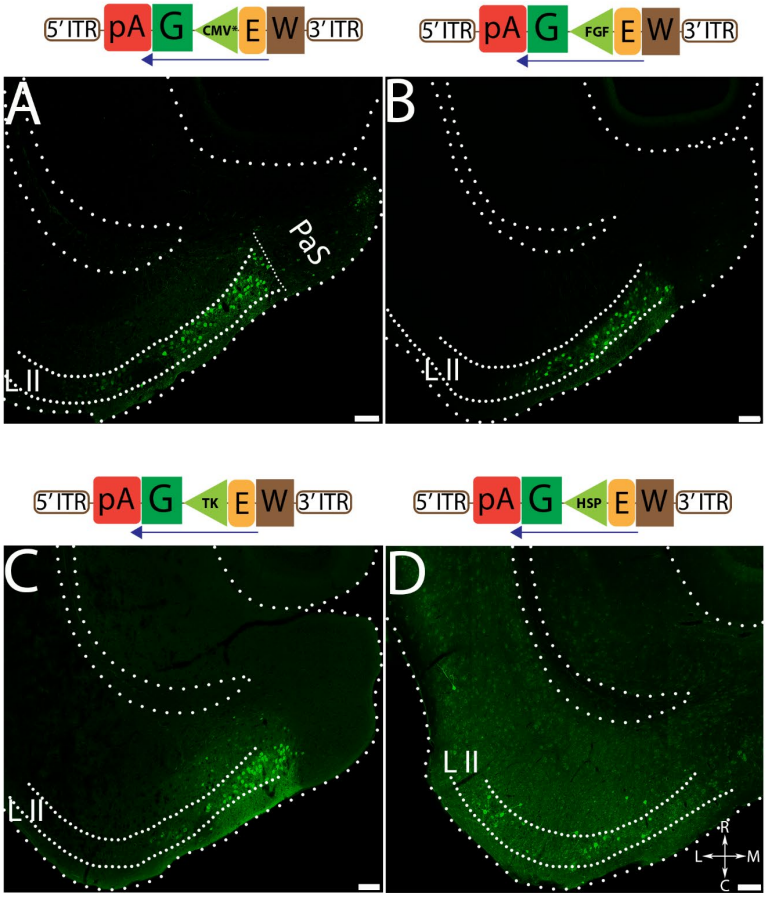
5′ITR
pA
G
CMV*
E
W
3′ITR
A
PaS
L II
5′ITR
pA
G
FGF
E
W
3′ITR
B
L II
5′ITR
pA
G
TK
E
W
3′ITR
C
L II
5′ITR
pA
G
HSP
E
W
3′ITR
D
L II
R
L
M
C

Figure S2. Optimization of minimal promoter for EDGE-rAAV constructs (related to Figure 1). *400 nl of MEC13-53 EDGE rAAVs with the various minimal promoters (A) CMV*, (B) FGF4, (C) TK or (D) HSP68 (see Methods for details) were injected into MEC in wild-type mice. While each minimal promoter led to layer-II specificity when combined with the MEC13-53 enhancer, we chose to use minimal CMV* because of its smaller size and limited nonspecific expression in other layers. Schematics of the viral designs are depicted on top of the corresponding image. See related supplemental Data S1 for sequences. Scale bar = 100 μm.*

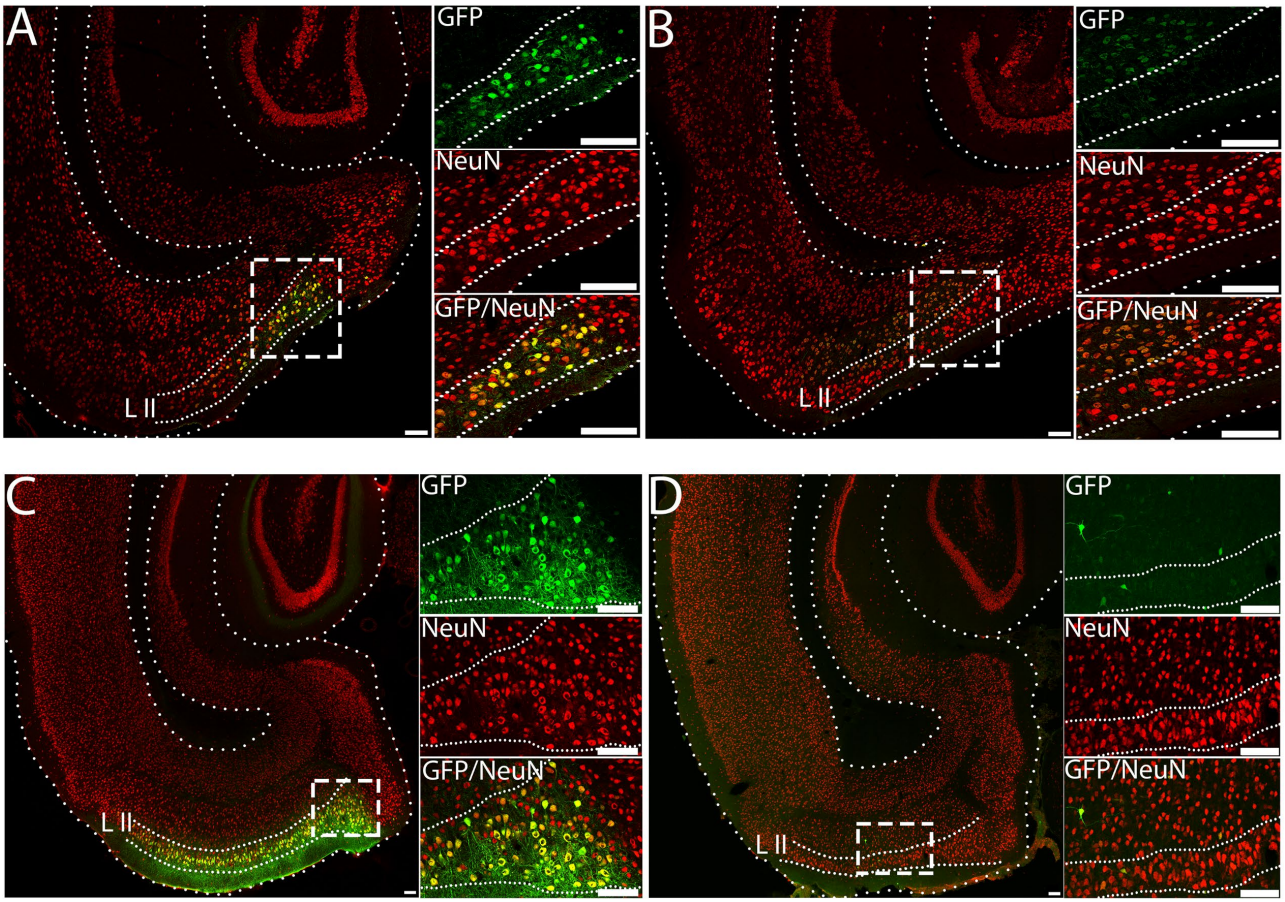
A
GFP
NeuN
GFP/NeuN
L II
B
GFP
NeuN
GFP/NeuN
L II
C
GFP
NeuN
GFP/NeuN
L II
D
GFP
NeuN
GFP/NeuN
L II

Figure S3. MEC13-53 drives transgene expression in LII MEC neurons (related to Figure 2). *Equal amounts of MEC13-53 rAAV (A, C) or CMV*-rAAV (B, D, i.e. identical to A except without an enhancer) were injected into MEC of wild-type mice (A, B) and rats (C, D). Insets show anti-GFP (top); NeuN marker (middle); and overlay (bottom) of box in main panel. Note the extensive co-localization of the NeuN stain with the GFP. Scale bar = 100 μm.*

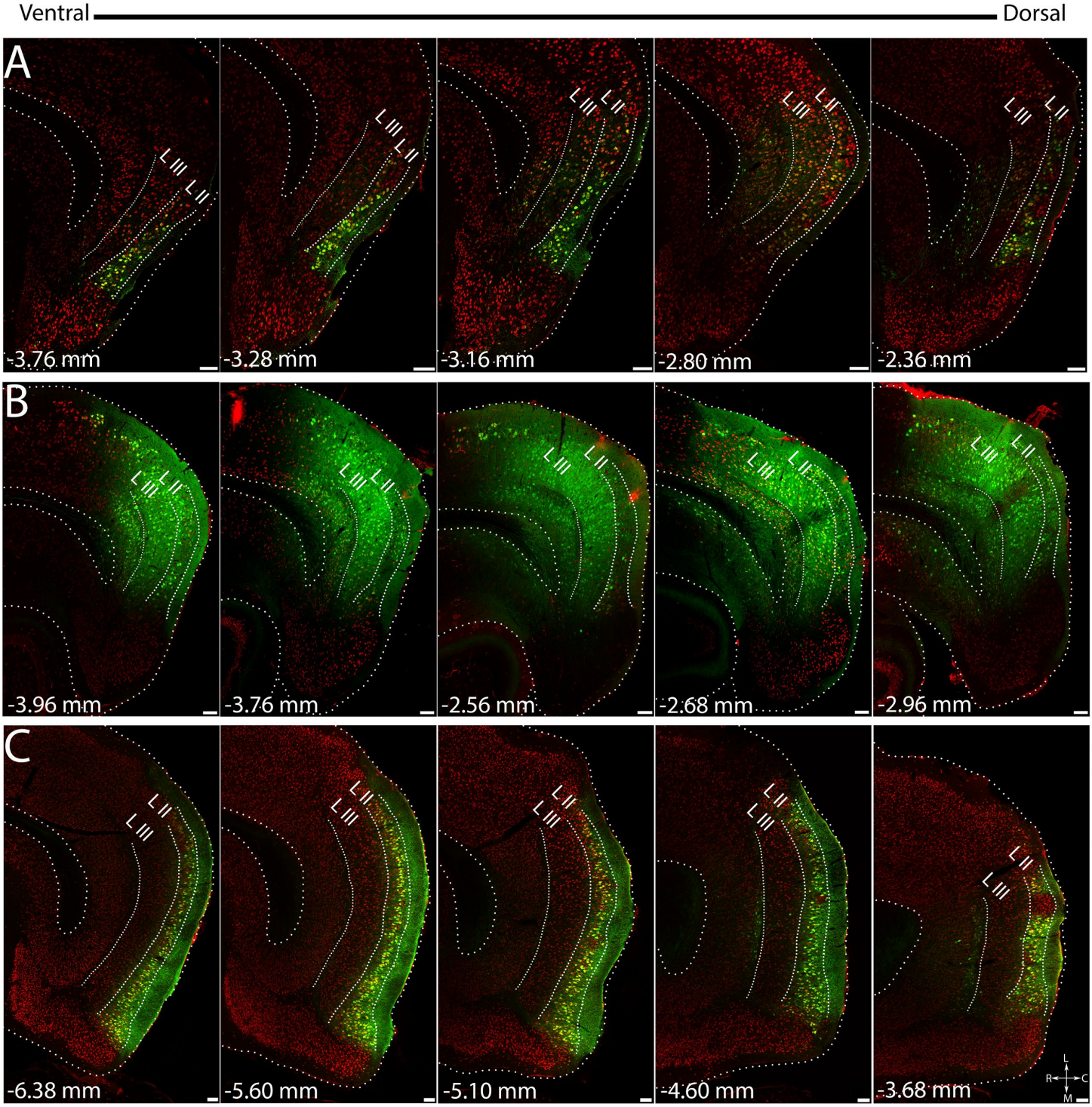
Ventral
Dorsal
A
L III
L II
-3.76 mm
-3.28 mm
-3.16 mm
-2.80 mm
-2.36 mm
B
-3.96 mm
-3.76 mm
-2.56 mm
-2.68 mm
-2.96 mm
C
-6.38 mm
-5.60 mm
-5.10 mm
-4.60 mm
-3.68 mm
L
R
C
M

Figure S4. EC LII specificity of MEC13-53 throughout the caudal forebrain (related to Figures 1 and 2). *Representative images of the GFP+ and NeuN+ neurons in horizontal sections at multiple dorso-ventral levels from, (A) a mouse brain injected with 400 nl and (C) a rat brain injected with 1000 nl of MEC13-53 rAAV. MEC13-53 drives transgene expression preferentially in MEC LII throughout dorso-ventral axis. (B) Representative images of the GFP+ and NeuN+ neurons in multiple horizontal sections in dorso-ventral axis from a mouse brain injected with CMV-rAAV. Label is throughout the layers of EC and also in subiculum. Sterotaxic coordinates were identified based on anatomical features using Paxinos G & Franklin K (for mouse brain) and Paxinos G & Watson C (for rat brain). Scale bar =100 µm.*

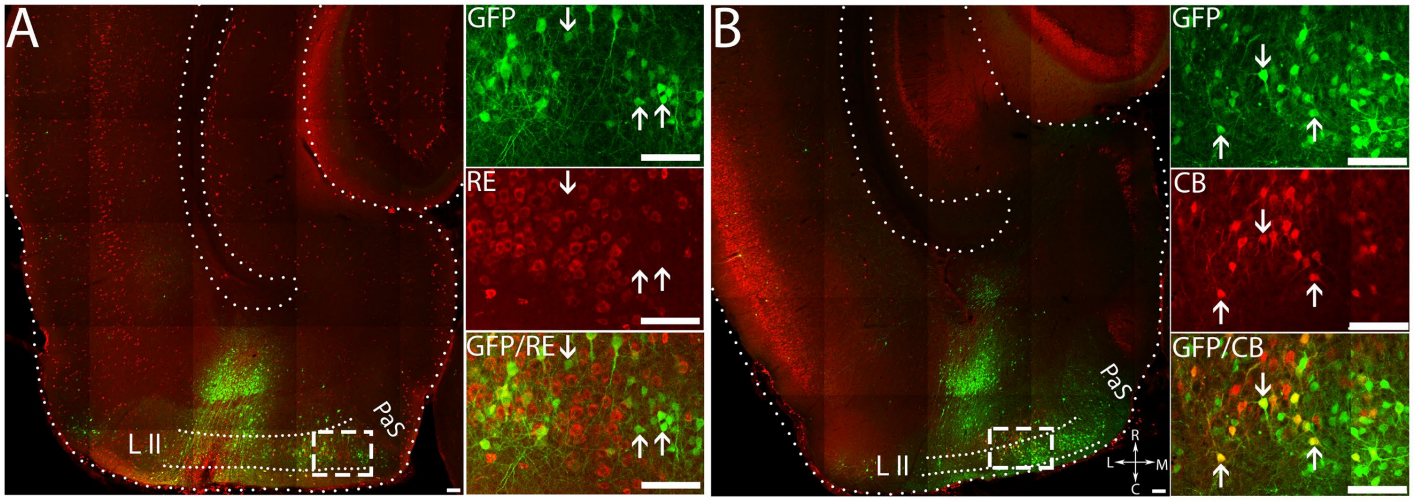
A
GFP
RE
GFP/RE
L II
PaS
B
GFP
CB
GFP/CB
L II
PaS
R
L
M
C

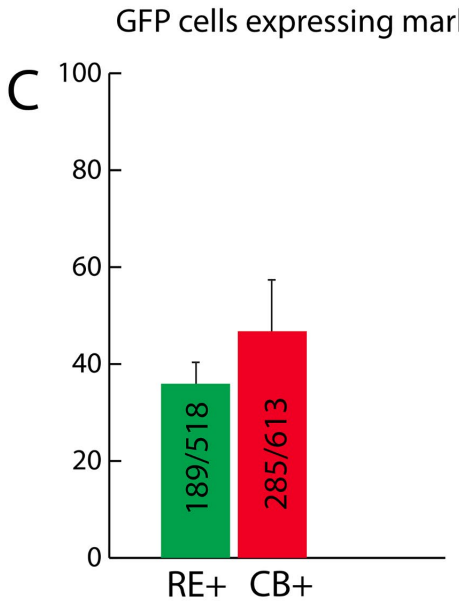
GFP cells expressing marker
C
100
80
60
40
20
0
189/518
285/613
RE+
CB+

Figure S5. CMV-rAAV is not specific to any cell-type in rat (related to Figure 2). *1000 nl CMV-rAAV was injected into MEC of wild-type rats. Insets show anti-GFP (top); marker (middle); and overlay (bottom) of box in main panel, marker is RE in A and CB in B. The arrows in A represent GFP+ cells that non-overlap with RE, while arrows in B show cells that are GFP+ and CB+. (C) Quantitation of results shown in A, B, showing 35 % overlap of GFP with cell-marker RE stain (green) in LII MEC, and 46 % overlap of GFP with CB (red), with number of cells counted. MEC-LII GFP+ cells were counted from separate RE and CB immunostained sections from 3 rats injected with CMV-rAAV, data represented as mean ± SEM. Scale bar = 100 μm.*

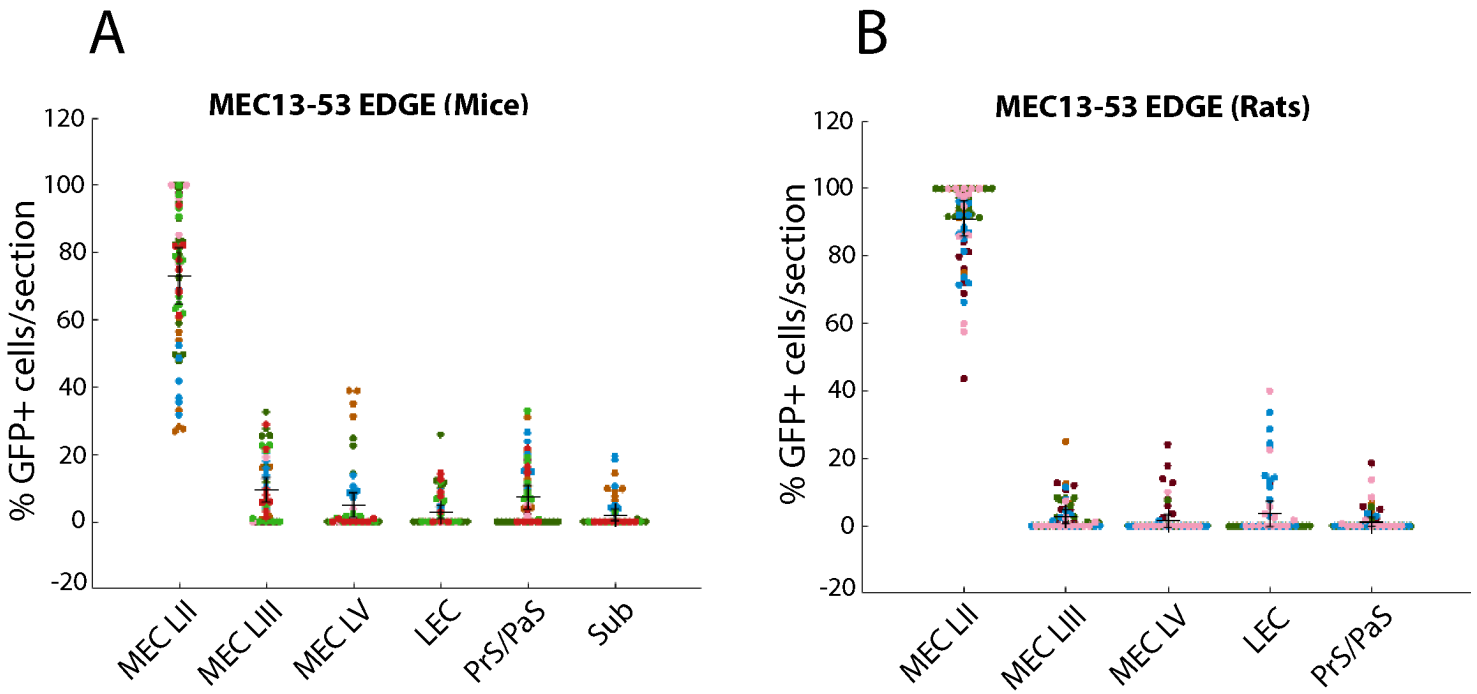
A
MEC13-53 EDGE (Mice)
% GFP+ cells/section
120
100
80
60
40
20
0
-20
MEC LII
MEC LIII
MEC LV
LEC
PrS/PaS
Sub
B
MEC13-53 EDGE (Rats)
% GFP+ cells/section
120
100
80
60
40
20
0
-20
MEC LII
MEC LIII
MEC LV
LEC
PrS/PaS

Figure S6. Layer II specific expression of MEC13-53 rAAV in multiple injections in two species (related to Figures 1 and 2). *MEC13-53 rAAV was injected into MEC of wild-type mice or rats. Sections were stained with anti-GFP, and GFP+ cells were counted in multiple sections per animal across various subdivisions of the parahippocampal area (see Transparent methods). The percentage of GFP+ cells/section analysed for different groups were plotted. (A, B) Distribution of percentage GFP+ cells/section across the different parahippocampal regions in all MEC13-53 EDGE injected mice (A) and rats (B). MEC13-53 rAAV LII sections with relatively few GFP+ cells are distal to the injection site). For (A) and (B) each colour represents the percentage GFP+ cells/section that belong to the same animal. The horizontal lines depict the mean percentage ± SEM.*

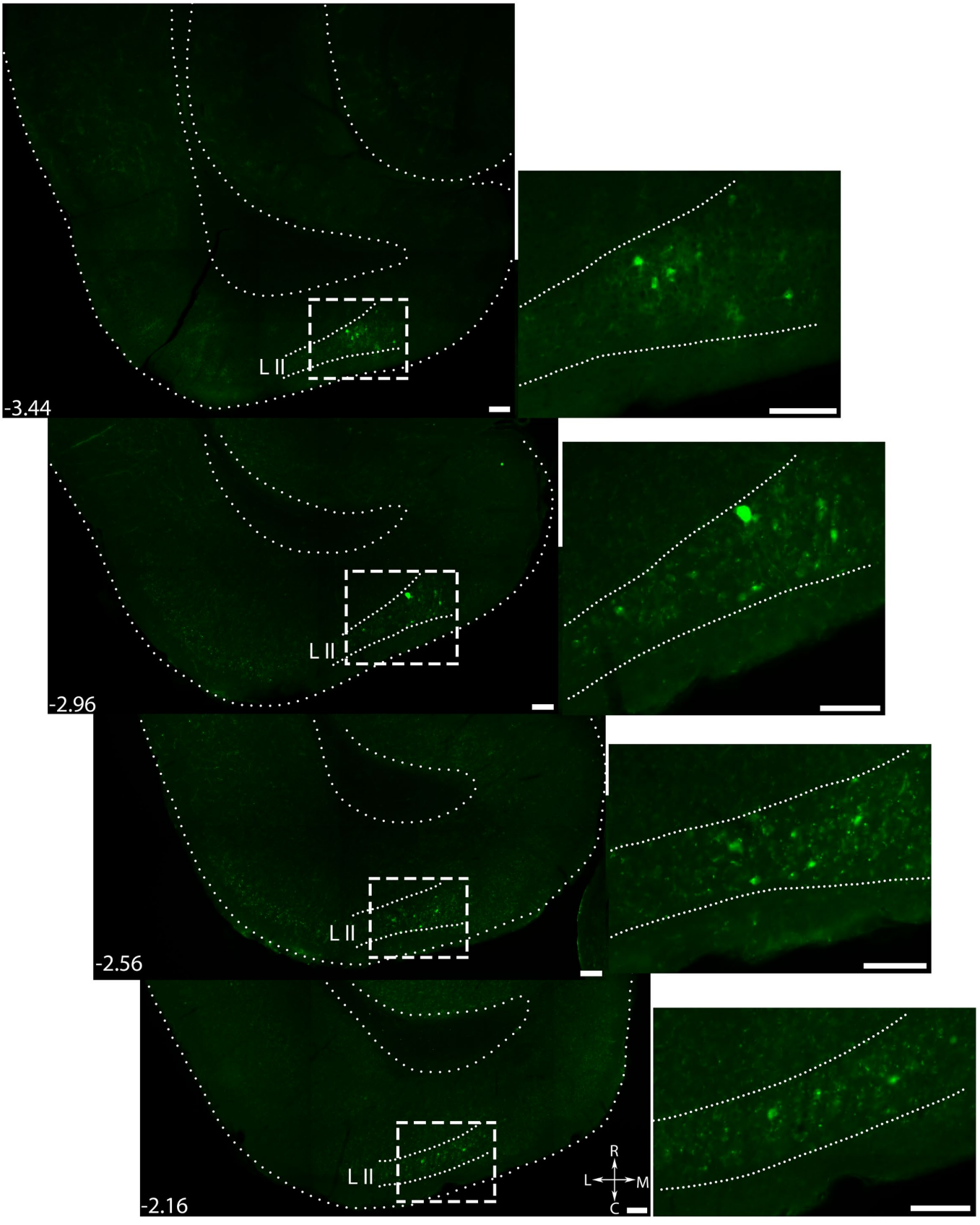
L II
-3.44
L II
-2.96
L II
-2.56
L II
-2.16
R
L
M
C

Figure S7. EC LII specificity of MEC13-53 rAAV PHP throughout the caudal forebrain (related to Figure 3). *Multiple dorso-ventral levels from the same mouse brain injected with MEC13-53 EDGE PHP into tail vein shows MEC13-53 drives transgene expression preferentially in MEC LII throughout dorso-ventral axis. Sterotaxic coordinates were identified based on anatomical features using Paxinos G & Franklin K (for mouse brain). See supplemental Table S2. Scale bar = 100 µm.*

Transparent Methods

79 **KEY RESOURCES TABLE**

80

81

REAGENT or RESOURCE	SOURCE	IDENTIFIER
Antibodies		
Rabbit anti-GFP	ThermoFisher Scientific	Cat# A-11122,RRID:AB_221569
Mouse anti-Reelin	Merck Millipore	Cat# MAB5364, RRID:AB_2179313
Mouse anti-Calbindin	Swant	Cat# 300, RRID:AB_10000347
Mouse anti-NeuN	Merck Millipore	Cat# MAB377, RRID:AB_2298772
Rabbit anti-2A peptide	Merck Millipore	Cat# ABS31, RRID:AB_10615498
Experimental models: Organisms/Strains		
C57BL/6J mice	Jackson laboratory	IMSR Cat# JAX:000664, RRID:IMSR_JAX:000664
Long Evans rats	Charles River	RGD Cat# 2308852, RRID:RGD_2308852
MEC13-53 tTA X tetO-TVAG	Blankvoort *et al* 2018	
MEC13-104 tTA X tetO-TVAG	Blankvoort *et al,* 2018	
LEC13-8 tTA X tetO-GCaMP6	Blankvoort *et al,* 2018	
AAV-293 cell line	Agilent	Cat# 240073 , CVCL_6871
Stbl3 *E. coli* strain	ThermoFisher Scientific	Cat# C737303

Reagents, chemicals, kits		
AAV helper free system	Agilent	Cat# 240071
pHelper	Agilent	Cat# 240071
pRC	Agilent	Cat# 240071
pXR1	NGVB, IU, USA	
pAAV PHP.B	Deverman *et al,* 2016	
Maxiprep kit	Qiagen	Cat# 12663
Fetal bovine serum	ThermoFisher Scientific	Cat# 16000-044
Benzonase nuclease HC	Merck Millipore	Cat# 71206-3
HiTrap® Heparin columns	GE	Cat# 17-0406-01
Amicon Ultra centrifugal filters	Merck Millipore	Cat# Z648043
Power SYBR™ Green PCR Master Mix	ThermoFisher Scientific	Cat# 4368577
DNase I	ThermoFisher Scientific	Cat# EN0521
DIG-labelled riboprobe	Roche	Cat# 11277073910
ISH blocking reagent	Roche	Cat# 11 096 176 001
Nitroblue tetrazolium chloride	Roche	Cat# 11 383 213 001
5-Bromo- 4-chloro- 3-indolyl-phosphate, 4-toluidene salt	Roche	Cat# 11 383 221 001
Levamisole	Vector	Cat# SP-5000

Instruments, softwares		
Confocal microscope, Zeiss LSM 880	Zeiss	
Zen 2012 software	Zeiss	
Hamilton needle	Hamilton	Cat# HAMI7762-06
Nanoliter injector, Nanoliter2010	World Precision Instruments	
Microsyringe pump controller, Micro4 pump	World Precision Instruments	
Axio Scan. Z1 scanner	Zeiss	
Zen 2.3 software	Zeiss	

CONTACT FOR REAGENT AND RESOURCE SHARING.

Further information and requests for resources and reagents should be directed to and will be fulfilled by the Lead Contact, Cliff Kentros (clifford.kentros@ntnu.no).

EXPERIMENTAL MODEL AND SUBJECT DETAILS

Rodent Details

Experiments were carried out using C57BL/6J mice (IMSR Cat# JAX:000664, RRID:IMSR_JAX:000664) obtained from Jackson laboratory, USA and Long Evans rats (RGD Cat# 2308852, RRID:RGD_2308852, Charles River, USA). EDGE transgenic crosses were created at the Kavli Institute for Systems Neuroscience and Centre for Neural Computation as described (Blankvoort et al., 2018). All experiments

were conducted in compliance with protocols approved by the Norwegian Food Safety Authorities and European Directive 2010/63/EU (FOTS ID 6269). All mice and rats were housed in enriched environment cages in a 12 hr light/dark cycle with food and water ad libitum.

METHODS DETAILS

Molecular cloning of constructs

All rAAV constructs were generated on backbone plasmid pAAV-CMV-MCS-WPRE-hGH PolyA (modified by cloning WPRE after the MCS in pAAV-MCS #240071, Agilent, USA). Control rAAV constructs were generated as follows: for ubiquitously expressing rAAV construct (CMV-rAAV) without a region-specific enhancer was generated by cloning the enhanced GFP (GFP) into the MCS of the pAAV-CMV-MCS-WPRE-hGH PolyA. For the promoterless construct for testing the transcriptional activity of ITRs, CMV promoter was removed from CMV-rAAV. To synthesize EDGE rAAV constructs, the CMV promoter, MCS and hGH PolyA sequences except WPRE were removed from pAAV-CMV-MCS-WPRE hGH PolyA. An expression cassette consisting of a hybrid promoter (composed of a region specific enhancer and minimal promoter), GFP and PolyA sequence were then subcloned into the plasmid in reverse orientation relative to the ITRs, to circumvent any promoter activity from the 5'ITR. The expression cassette in the reverse orientation was cloned into the plasmid upstream of the WPRE which thus minimized the promoter activity from the 3'ITR. Various EDGE rAAV constructs with the revised design were generated by cloning murine enhancers obtained from our initial enhancer screen such as MEC-13-53, MEC-13-104 or LEC-13-8 and different minimal core promoters: a variant of CMV (CMV*, derived from the sequence of pTRE3G, Clontech, USA) (Loew et al., 2010), fibroblast growth factor 4

(FGF4) (Murtha et al., 2014), HSV-TK (sequence from NEB, USA) or HSP68 (Blankvoort et al., 2018, Cotney et al., 2013) into the expression cassette in the reverse orientation. Sequences of the EDGE rAAVs, the region specific enhancers and the minimal promoters used in the study are given below. Plasmids were maintained in the Stbl3 *E. coli* strain (#C737303, ThermoFisher, USA) to avoid ITR-mediated recombination. Enhanced GFP, WPRE, LEC-13-8 and minimal promoters were synthesized by Genscript, USA. Positive clones were confirmed by restriction digestion analyses and subsequently by DNA sequencing. Endotoxin-free plasmid maxipreps (#12663, Qiagen) were made for rAAV preparations.

rAAV preparations

EDGE rAAVs were packaged in AAV serotype 2/1 (having a mosaic of capsid 1 and 2) (Hauck et al., 2003) using Heparin column affinity purification (McClure et al., 2011). Specifically, a pAAV construct generated as described above with AAV helper plasmids encoding the structural elements, were transfected into the AAV-293 cell line (CVCL_6871, Agilent, USA). The day before transfection, 7 x 10^6 AAV-293 cells were seeded into 150 mm cell culture plates in DMEM containing 10% fetal bovine serum (#16000-044, ThermoFisher, USA) and penicillin/streptomycin. Co-transfection of plasmids such as pAAV-containing the transgene, pHelper, pRC (#240071, Agilent, USA) and pXR1 (NGVB, IU, USA) was carried out next day. After 7 hours, the medium was replaced with fresh 10% FBS-containing DMEM. The AAV-293 cells were cultured for two days following transfection to allow rAAV synthesis to occur. The AAV-293 cells filled with virus particles were scraped from the cell culture plates, then isolated by centrifugation at 200 x g. The cell pellet was then subjected to lysis using 150 mM NaCl-20 mM Tris pH 8 buffer containing 10 % sodium deoxycholate. The lysate was treated with benzonase nuclease HC (#71206-3, Millipore) for 45 minutes at 37^{o}C.

Benzonase-treated lysate was centrifuged at 3000 x g for 15 mins and the clear supernatant then subjected to HiTrap® Heparin High Performance (#17-0406-01, GE) affinity column chromatography using a peristaltic pump (McClure et al., 2011). The elute from the Heparin column was concentrated using Amicon Ultra centrifugal filters (#Z648043, Millipore). The titer of the resultant viral stock was determined by quantitative PCR as approximately 10^{11} infectious particles/ml.

EDGE rAAVs were packaged in AAV PHP.B and purified using iodixanol density gradient method. Specifically, pAAV construct was transfected into the AAV-293 cell line (CVCL_6871, Agilent, USA) along with AAV helper plasmids encoding the structural elements. The day before transfection, 7 x 10^6 AAV-293 cells were seeded into 150 mm cell culture plates in DMEM containing 10% fetal bovine serum (#16000-044, ThermoFisher, USA) and penicillin/streptomycin. PEI mediated co-transfection of plasmids such as pAAV-containing the transgene, pHelper, pAAV PHP.B (Deverman et al., 2016) was carried out next day. After 24 hours, the medium was replaced with fresh 10% FBS-containing DMEM. The AAV-293 cells were cultured for two days following transfection to allow rAAV synthesis to occur. The medium and AAV-293 cells filled with virus particles were scraped from the cell culture plates, then isolated by centrifugation at 200 x g. The cell pellet was then subjected to lysis using 20 mM Tris, 300 mM NaCl and 20 mM $MgCl_2$, pH 7.6 buffer. The supernatant was mixed with 40% PEG for 2 hours in ice for precipitation of virus particles. Centrifuge the PEG treated medium at 4000 x g for 15 minutes. The lysate and the PEG-precipitate was treated with benzonase nuclease HC (#71206-3, Millipore) for 45 minutes at 37ºC. Benzonase-treated lysate was centrifuged at 3000 x g for 15 mins and the clear supernatant then subjected to iodixanol gradient ultracentrifugation. 4 different layers of the gradient, i.e. 15%, 25%, 40%, and 58% of iodixanol was built in a Beckman and

Coulter quick-seal centrifuge tube. Phenol red was added to the 25% and 58% layers to aid visualization of the layers within the tube. The virus containing supernatant was layered above the 15% iodixanol by slowly dripping the solution onto the top layer of the gradient. Seal the tip of the tube using a heating device (Beckman and Coulter). The 40% iodixanol layer, after ultracentrifugation at 200,000 g for 2 hours at 18^{o}C, was collected and buffer exchanged with DPBS using Amicon Ultra centrifugal filters (#Z648043, Millipore) (modified protocol from Addgene, USA).

Titration of the rAAVs

The titration of the rAAVs prepared for the study was carried out by quantitative PCR (Aurnhammer et al., 2012, Gray et al., 2011) using Power SYBR™ Green PCR Master Mix (#4368577, ThermoFisher, USA), the following primers were used for GFP; forward primer- 5'-AGCAGCACGACTTCTTCAAGTCC and reverse primer 5'-TGTAGTTGTACTCCAGCTTGTGC (modified protocol from Addgene, USA). A known concentration (2 x 10^9 molecules/µl) of a pAAV construct containing the GFP sequence was used for generating the standard curve. 5 serial dilutions of plasmid from 2 x 10^8 to 2 x 10^5 were made in PCR grade water for creating the standard curve. The purified rAAVs were treated with DNase I (#EN0521, ThermoFisher, USA) at 37^{o}C for 30 minutes, to eliminate any contaminating plasmid DNA carried over from the rAAV production process. DNAse-treated rAAVs were serially diluted for the qPCR titration (from 1:20 to 1:2500) in PCR grade water. A mastermix of the reagents for the qPCR was prepared consisting of the SYBR Green PCR Master Mix, the primers and PCR-grade water. 5µl each from the standards and the rAAV dilutions along with 15µl of mastermix were subjected to qPCR at 95^{o}C 10 min / 95^{o}C 15 sec / 60^{o}C 1 min/ repeat 40x/ melt curve using StepOne machine (Applied Biosystems, USA). Data analyses were performed by StepOne2.3 software and by Microsoft excel.

Stereotaxic Injections

For rat experiments, the rAAVs were stereotactically injected into three-four months old male Long-Evans rats. Injections were performed with 1 µl rAAV at a titer of ~1 x10^{11} infectious particles/ml, into the MEC of the rats. The rats were deeply anaesthetized with isoflurane gas (induction with 5 % isoflurane (v/v), maintenance at 1 % isoflurane (v/v), airflow of 1200 ml/min). To maintain the body temperature of the animal, a heating pad at 37^{o}C was used.

Rats were injected subcutaneously with buprenorphine hydrochloride (Temgesic®, Indivior) and Metacam® (Boehringer Ingelheim Vetmedica) at the prescribed dosage. Local anaesthetic Bupivacaine hydrochloride (Marcain^{TM}, AstraZeneca) was applied at the place of incision. The head was fixed to the stereotaxic frame with ear bars, and the skin at the incision site was disinfected with 70 % ethanol and iodine before the incision was made using a sterile surgical scalpel blade. After incision, the mouthpiece and ear bars were adjusted so that bregma and lambda were aligned horizontally. Mediolateral coordinates were measured from the mid-sagittal sinus, anterior-posterior coordinates were measured from posterior transverse sinus, and dorso-ventral coordinates were measured from the surface of the brain. A craniotomy was made around the approximate coordinate, and precise measurements were made with the glass capillary/Hamilton needle (HAMI7762-06) used for virus injection. Coordinates for rat injections were 4.6 mm lateral, 0.2 mm anterior to the posterior transverse sinus and 2.6 mm deep, with the glass capillary/needle lowered at 10^{o} pointing towards the nose. A single injection of 1 µl virus was conducted at a speed of 100 nl/min using a nanoliter injector (Nanoliter2010, World Precision Instruments, Sarasota, FL, USA), controlled by a microsyringe pump controller (Micro4 pump, World Precision Instruments). After completion of the injection, the capillary was

retracted after a 10 minutes delay, to give the virus time to diffuse. Finally, the wound was rinsed with saline and the skin was sutured. The animals were left to recover in a heating chamber, before being returned to their home cage. Next day Metacam was administered orally and their health was checked daily.

For mouse experiments, 10-15 weeks-old adult C57BL/6J mice (male or female) were anaesthetized with isoflurane (induction with 5 % isoflurane (v/v), maintenance with 1 % isoflurane (v/v), airflow of 1200 ml/min). After applying the local analgesic Marcain (40 µl, 0.25 mg/ml, SC), the global analgesic Temgesic (0.03 mg/ml, 100-150 µl per mouse dependent on bodyweight, SC), and Metacam (2.5 mg/ml, 100-150 µl per mouse dependent on bodyweight, SC) the head was fixed in a stereotaxic frame. Subsequently the skull was exposed by a single incision of the scalp, craniotomies were made approximately 5 mm posterior and 3.3 mm lateral of the bregma. Then, the virus solution was injected at a location 0.3-0.5 mm anterior to the transverse sinus and at a depth of 1.8-2.0 mm from the brain surface. Unless otherwise stated, all injections were bilateral injections of 400 nl rAAV injected at a rate of 50 nl/min. Mice were given a second post-operative injection of Metacam the next day, and their weight was monitored until stable.

Tail vein injections

For tail vein injections, 10-15-weeks-old adult C57BL/6J mice (male or female) were anaesthetized with isoflurane (induction with 5 % isoflurane (v/v), maintenance with 1 % isoflurane (v/v), airflow of 1200 ml/min). Anaesthetized mouse was placed on a heat pad maintained at 37 ^{o}C during the procedure. The tail was wiped using 70% alcohol and warmed using water pad to cause vasodilation of the vein. Mice were injected with EDGE rAAV PHP virus preparation into lateral tail vein to a total volume of 100 µl in PBS (approx. 1 x 10^{12} infectious particles/mouse) using a 30-gauge insulin syringe

(#720-2555, Omnican, B.Braun). Remove the needle from the vein and apply slight pressure to the puncture site with a dry piece of sterile cotton until the bleeding has stopped.

Perfusions

After 4 weeks, the rodents were sacrificed. Rodents were anaesthetized with pentobarbital and perfused transcardially with freshly prepared 0.9 % saline followed by 4 % paraformaldehyde in 0.1 M Phosphate buffer (pH 7.4) with 0.9 % saline. The brains were stored in 4% PFA overnight before being transferred to 30% sucrose solution for approximately two days.

Immunostaining

Horizontal rat brain sections of 50 µm were prepared using a sliding microtome at -30^{o}C. Brain sections were stored at -20^{o}C in 0.1 M phosphate buffer containing 25 % glycerin and 30 % ethylene glycol. Multiple labelling of free-floating sections was carried out as briefly described. Usually, every sixth section in the series was selected for immunostaining and washed in phosphate-buffered saline (PBS). Sections were permeabilized and blocked for 1 hour at room temperature using PBS containing 0.1 % Triton X-100 and 3 % normal donkey serum, or, when staining for reelin and calbindin 0.5 % Triton X-100 and 5 % goat serum and when staining for NeuN 0.3 % Triton X-100 and 3 % BSA (PBS++). Sections were subsequently incubated with primary antibodies in PBS++ at 4^{o}C for two days with mild shaking. PBS-washed sections were incubated for 2 hours at room temperature with secondary antibodies diluted in PBS++ (or PBS containing Triton X-100 without serum/BSA).

Solution containing 2.5 % 1,4-diazabicylo[2.2.2]octane/polyvinyl alcohol (DABCO/PVA) was used to mount the sections in Polysine slides (Menzel-Glaser, ThermoFisher, USA). Antibodies used were rabbit anti-GFP (Thermo Fisher Scientific

Cat# A-11122, RRID:AB_221569, 1:500), mouse anti-Reelin (Merck Millipore Cat# MAB5364, RRID:AB_2179313, 1:1000), mouse anti-Calbindin (Swant Cat# 300, RRID:AB_10000347, 1:5000), mouse anti-NeuN (Millipore Cat# MAB377, RRID:AB_2298772, 1:1000) and rabbit anti-2A peptide (Millipore Cat# ABS31, RRID:AB_10615498, 1:2000). All corresponding secondary antibodies were from ThermoFisher/Life technologies or Jackson ImmunoResearch laboratories, USA, used at a dilution of 1:400.

In situ hybridization

Mice were perfused transcardially with 4% paraformaldehyde (PFA) in RNAse free PBS. The brain was extracted and stored in 4% PFA overnight before being transferred to 30% RNAse free sucrose solution for approximately two days. The brain was then sectioned horizontally in 30 µm thick sections and divided into a set of approximately 6 series and stored in a -80^{o}C freezer. A series was then thawed before use. To stain transgenes TVAG or HM3, 30µm thaw-mounted sections were hybridized overnight at 62^{o}C with a DIG-labelled riboprobe for TVAG or HM3 (approximately 1:500; Roche, Cat. 11277073910) and then incubated in Blocking solution (600µl MABT, 200µl sheep serum, 200µl 10% blocking reagent (Roche, Cat. No. 11 096 176 001) for 2-3 hours at room temperature. Slides were drained of the blocking solution, and antibody solution (1:5000 dilution of sheep anti-dig alkaline-phosphatase (AP) in blocking solution) was added to the slides. The slides were transferred back to the Perspex box and incubated at room temperature overnight. 4g of polyvinyl alcohol (Mol. Wt. 70000 – 100000) were transferred to a 50ml polypropylene centrifuge tube, and AP staining buffer (100mM NaCl, 50mM $MgCl_2$, 100mM Tris pH 9.5, 0.1% Tween-20) was added till the total volume of the solution was 40 ml. The solution was shaken to dissolve the solid material, and further heated

in a water bath. When the solution was clear, it was cooled down to 37°C. The slides were washed 5 times in MABT in room temperature for 4 min each wash. Further, the slides were washed 2 times in AP staining buffer for 10 min in room temperature while the slides were shaken. NBT (Nitroblue tetrazolium chloride, Roche. Cat. No. 11 383 213 001, 140 µl/40ml), BCIP (5-Bromo- 4-chloro- 3-indolyl- phosphate, 4-toluidene salt, Roche, Cat. No. 11 383 221 001, 105 µl/40 ml) and Levamisole (Vector, Cat. No. SP-5000, 3.2ml/40ml) were added to the polyvinyl alcohol solution, and mixed well before transferring it to a Coplin jar together with the slides. The slides were incubated at 37°C for 5 hours. After incubation, the slides were washed 2 times in PBS + 0.1% Tween-20 to stop the staining reaction. The slides were further washed 2 times in ddH_2O and left air dry at room temperature for overnight. The slides were cleared in xylene and coverslipped. The stained sections were imaged using automated Axio Scan. Z1 scanner (Zeiss), Zen 2.3 software with transmitted white light as the light source.

QUANTIFICATION AND STATISTICAL ANALYSIS

Confocal Imaging and Analysis

Brain sections were imaged using a confocal microscope (Zeiss LSM 880, Zen 2012 software) with either Plan-Apochromat 40x/1.4 Oil DIC M27 oil immersion or Plan-Apochromat 20x/0.8 air immersion objectives. Image acquisition was done at identical capture settings in confocal microscope. Captured images were processed identically using Zen 2012 software and figures were prepared using Adobe photoshop. Confocal images of GFP expression for different viral constructs were captured using 488nm laser. For figure S1, identical post-acquisition processing for the purposes of comparison of strong versus weak viral GFP expression seen with the different viral

constructs, was carried out as explained below. Confocal images (czi.) were opened in Zen 2012 software. Intensity range indicator tool was used to visualize, and display tab was used modify the brightness intensity level of the acquired image. The brightness intensity levels for the green channel was modified until the optimum intensity was attained, as displayed by the range indicator. Once the parameters for the optimal brightness intensity for green channel for one viral construct was identified, identical changes in the intensity levels were applied to the other identically captured confocal images for strong versus weak viral GFP expression comparison (Figure S1). For e.g. in 2nd row (D-F) in Figure S1, the optimal intensity parameters for visualizing D was determined using range indicator and display tab and subsequently applied identically to the E and F.

The quantification of GFP+, NeuN+, RE+ or CB+ cells was performed out manually using Zen 2012 software. Approximately ten 50 µm thick horizontal sections were selected from the dorso-ventral axis (-1.5 mm to -4 mm from Bregma) per brain. Counts were carried out on the confocal images (.czi format) of rAAV injected brain sections immunostained for GFP or respective markers (NeuN, RE, CB). For the layer specificity analyses shown in Figure 2C, 13096 (3 mice) and 8540 GFP+ cells (7 mice) were counted from mice, injected with CMV-rAAV and MEC13-53 rAAV respectively. Data about MEC13-53 rAAV injections in mice includes counts from two different batches of the MEC13-53 rAAV. Any fluorescent signal greater than background auto-fluorescence was considered as positive, even though there was often a baseline transcription from the rAAV promoter construct versus the enhancer-assisted (EDGE) signal, which was typically orders of magnitude greater. For analyses in rat brains (Figure 2G), 7191 GFP+ cells from sections were counted from 76 horizontal sections from 5 separate hemispherical injections of MEC13-53 rAAV in 3 rats (-2 mm to -6 mm

342 from Bregma) and 2831 GFP+ cells were counted for CMV-GFP. For the quantification
343 of MEC-LII EDGE GFP cells expressing cell-markers, 2406 (RE co-immunostained)
344 and 1668 (CB co-immunostained) GFP+ cells were counted from 7 separate MEC13-
345 53 rAAV injected mice (Figure 2D). For similar analyses in rats (Figure 2H), 2332 and
346 1799 MEC-LII GFP+ cells were counted from separate RE and CB immunostained
347 sections from 5 different hemispherical injections of MEC13-53 rAAV (we analysed 31
348 sections for RE and 27 sections for CB) from 3 rats. Analyses were done in Microsoft
349 excel and graphs were made in Adobe illustrator. For the supplemental figure S6,
350 plotspread toolbox of Matlab was used to represent individual measurements of each
351 tissue section analysed per animal and per group. For the statistical analysis of the
352 percentage of GFP positive cells, we used SPSS software. For the comparison of the
353 means, One-way ANOVA test was used and LSD Post Hoc test was conducted with
354 a significant level of 0.01.

355

Supplemental References

AURNHAMMER, C., HAASE, M., MUETHER, N., HAUSL, M., RAUSCHHUBER, C., HUBER, I., NITSCHKO, H., BUSCH, U., SING, A., EHRHARDT, A., et al. 2012. Universal real-time PCR for the detection and quantification of adeno-associated virus serotype 2-derived inverted terminal repeat sequences. *Hum Gene Ther Methods,* 23**,** 18-28.

BLANKVOORT, S., WITTER, M. P., NOONAN, J., COTNEY, J. & KENTROS, C. 2018. Marked Diversity of Unique Cortical Enhancers Enables Neuron-Specific Tools by Enhancer-Driven Gene Expression. *Curr Biol,* 28**,** 2103-2114 e5.

COTNEY, J., LENG, J., YIN, J., REILLY, S. K., DEMARE, L. E., EMERA, D., AYOUB, A. E., RAKIC, P. & NOONAN, J. P. 2013. The evolution of lineage-specific regulatory activities in the human embryonic limb. *Cell,* 154**,** 185-96.

DEVERMAN, B. E., PRAVDO, P. L., SIMPSON, B. P., KUMAR, S. R., CHAN, K. Y., BANERJEE, A., WU, W. L., YANG, B., HUBER, N., PASCA, S. P., et al. 2016. Cre-dependent selection yields AAV variants for widespread gene transfer to the adult brain. *Nat Biotechnol,* 34**,** 204-9.

GRAY, S. J., CHOI, V. W., ASOKAN, A., HABERMAN, R. A., MCCOWN, T. J. & SAMULSKI, R. J. 2011. Production of recombinant adeno-associated viral vectors and use in in vitro and in vivo administration. *Curr Protoc Neurosci,* Chapter 4**,** Unit 4 17.

HAUCK, B., CHEN, L. & XIAO, W. 2003. Generation and characterization of chimeric recombinant AAV vectors. *Mol Ther,* 7**,** 419-25.

LOEW, R., HEINZ, N., HAMPF, M., BUJARD, H. & GOSSEN, M. 2010. Improved Tet-responsive promoters with minimized background expression. *BMC Biotechnol,* 10**,** 81.

MCCLURE, C., COLE, K. L., WULFF, P., KLUGMANN, M. & MURRAY, A. J. 2011. Production and titering of recombinant adeno-associated viral vectors. *J Vis Exp***,** e3348.

MURTHA, M., TOKCAER-KESKIN, Z., TANG, Z., STRINO, F., CHEN, X., WANG, Y., XI, X., BASILICO, C., BROWN, S., BONNEAU, R., et al. 2014. FIREWACh: high-throughput functional detection of transcriptional regulatory modules in mammalian cells. *Nat Methods,* 11**,** 559-65.